PET Electron Calibrations

SRL technical report #93-1

Richard Selesnick

November 1, 1993

This is a report on the results of the Proton/Electron Telescope (PET) electron calibrations and on a preliminary analysis of flight electron data. It is intended to provide a starting point for more detailed studies by summarizing the PET electron response characteristics, illustrating their application to data analysis, describing various difficulties and anomalies encountered to date, and suggesting some possible future refinements.

Memoranda by myself (10/31/91) and Dick Mewalt (11/17/91), describing the calibration procedures and experimental setups used at the SRL β-spectrometer and at the the EG&G linear electron accelerator in Santa Barbara respectively, are included in the PET user's document. The two facilities were required to cover most of PET's useful energy range. They also provided a cross check because the energy ranges of each calibration, ~0.3 to 3 MeV for the β-spectrometer and ~1.5 to 27 MeV for the accelerator, had some overlap. Angles of incidence of the electron beam relative to the telescope axis varied from 9° to 90° for the β-spectrometer and 0° to 80° for the accelerator. All of the detectors and guards were instrumented to record pulse heights at the accelerator, while only the front three plus guard (P1, P2, P3, A3) were instrumented at the β-spectrometer due to the lower energy range. The SRL Macsys data collection system was used for both calibrations and various characteristics of the flight electronics, such as energy thresholds and coincidence equations, were added later by software. This provides for a fairly simple re-analysis of the calibration data in case the electronic characteristics are revised.

Both calibration and flight data from PET consist of the number of counts N_{ik} recorded in each channel i of each event type k. The PET event types (defined in the user's document) correspond to the rate counters: ELO, EHI, PLO, PHI, RNG, EWG, and PEN. Those of primary interest for electrons are ELO and EHI, with the possible inclusion of RNG and EWG for higher energies. The channels for each event type may correspond directly to the ADC channels or to some linear combination of them. In the analysis to date I have used a linear combination that leads to channel numbers that are approximately proportional to the total electron energy, as described below. The data are recorded over a certain real time interval Δt, but the instrument livetime τ_k during this interval is generally shorter due to deadtime and to the event buffering scheme, and may vary with event type k. For flight data

$$\tau_k = \frac{N_k^{PHA}}{N_k^{RATE}} \frac{PLIVE}{734.15} (6 \text{ s}) \tag{1}$$

where $PLIVE$ is the total number recorded by the livetime rate counter during Δt (which should be a multiple of the 6 s rate accumulation period), N_k^{PHA} is the total number of pulse height analyzed events satisfying event type k, and N_k^{RATE} is the number of counts from the type k rate counter. Note that the fraction of analyzed events, N_k^{PHA}/N_k^{RATE}, should always be less than or equal to 1, but for rare cases in the flight data it is actually greater than 1. This is not currently understood and I have chosen to set it equal to 1 in these cases. In the calibrations all events were recorded and the livetime is also recorded directly by Macsys.

The relationship between N_{ik} and the electron intensity, j, defines the response functions R_{ik}:

$$N_{ik} = \tau_k \int_0^{2\pi} \int_0^{\pi} \int_0^{\infty} R_{ik}(E,\theta)\ j(E,\alpha(\theta,\phi))\ dE\ \sin\theta\ d\theta\ d\phi \tag{2}$$

where θ and ϕ are spherical angles relative to the telescope axis. For flight data j may depend on the electron pitch-angle α relative to the magnetic field as well as the incident kinetic energy E. In these cases α must be related to θ and ϕ, as in eq. (2), by

$$\sin^2\alpha = \sin^2\theta[\sin^2\phi + (\cos\phi\cos\theta_B - \cot\theta\sin\theta_B)^2] \tag{3}$$

where θ_B is the angle between the magnetic field and the telescope axis. However, the analysis is greatly simplified for an isotropic distribution (j depends only on E) and I assume this for the analysis of flight data. For calibration data j depends directly on E, θ and ϕ:

$$j = J_n \delta(E - E_n) \frac{\delta(\theta - \theta_n)}{\sin\theta} \delta(\phi - \phi_n) \tag{4}$$

where J_n is the beam flux density (electrons/cm^2-s) and the subscript n refers to beam parameters for the nth calibration run. The $\sin\theta$ is required so that $\int j d\Omega = J_n$. Since we assume that R_{ik} is independent of ϕ, the beam azimuthal direction ϕ_n is not significant.

Different methods were required to determine J_n for the β-spectrometer and accelerator due to the different setups. At the β-spectrometer a single 4.5 cm^2 detector was placed in the beam to measure J_n directly for each E_n. The detector was also moved horizontally at a fixed E_n to determine the spatial uniformity of the beam and the best location for PET. A contour map and 3-d representation of the measured beam profile are shown in Figure 1. Details of the method for determining the map are given in SRL internal report #100. Since position measurements of individual electrons were not made it is not possible to correct for the non-uniformity of the beam, which therefore introduces small systematic errors into the results. The values of J_n measured with the 4.5 cm^2 detector centered at the location shown in Figure 1 were used, providing an average beam flux over this area. It would perhaps have been somewhat more accurate to use the beam map to find the average flux over the 8 cm^2 area of the P1 detector. At the accelerator position measurements were made by the multi-wire proportional counter (MWPC). This turned out to be essential because the beam was highly non-uniform at high energies. For data analysis the MWPC area was divided into a grid and the number of events from each grid square were then separately normalized by the flux through that square. A 20×20 grid was found to provide accurate results. Details of this method are given in SRL internal report #79.

The calibration analysis consists of determining $R_{ik}(E,\theta)$ given N_{ik} and j, while the flight data analysis consists of determining $j(E)$ given N_{ik} and R_{ik}. Since R_{ik} and j are both inside the integral in eq. (2), similar methods can be used. (Alternatively, the calibration and flight data could be used to simultaneously determine R_{ik} and j from eq. (2).) However, with j from eq. (4) the integrals in eq. (2) can be done easily and

$$R_{ik}(E_n,\theta_n) = \frac{N_{ik}}{\tau_k J_n} \tag{5}$$

The results of this calculation are shown in Figure 2 for P1 singles events (i.e., a P1 trigger is the only requirement). There are 112 runs from the β-spectrometer and 143 runs from the accelerator included at various angles and energies. These data are summed over all channels, k, so that they are appropriate to the P1 counting rate. While the β-spectrometer results appear fairly regular, there is some scatter in the accelerator data that is not accounted for by the statistical error bars. In addition there is a discrepancy between the two calibrations in the region of energy overlap. This is probably a results of some divergence in the electron beam due to scattering in the beam pipe exit window and in the intervening material between it and PET (including some air, a helium bag, and the MWPC). By estimating the mean scattering angle and modifying eq. (4) accordingly (e.g. by replacing the directional δ-functions with Gaussians), the scattering could be taken into account, but currently I have not attempted this. Instead, I have renormalized the accelerator data by multiplying each point by the ratio of the β-spectrometer and accelerator results at 0° (actually the β-spectrometer data were only available at 9° so these were divided by cosθ = 0.988). At energies above those available from the β-spectrometer the accelerator data were multiplied by the ratio of 8 cm^2, the actual area of P1, and the accelerator results at 0°. There is therefore a set of correction factors, each of which applies to all of the runs at different angles for a given accelerator beam energy. These corrections factors vary from 0.84 to 1.21. The results are shown in Figure 3. The same set of correction factors (i.e., those derived from the P1 singles events) were applied to all event types and the results are shown for ELO and EHI in Figures 4 and 5 respectively, again summed over all channels.

The results in Figures 3, 4, and 5 still are clearly effected by some remaining systematic errors as well as statistical errors. In addition, they are only available at the beam energies and angles. It is therefore useful to do some smoothing and interpolation. There are many possible ways to do this, all of which are difficult to justify because they involve some more or less arbitrary assumptions. However, we have to choose one because the integrals in eq. (1) require R_{ik} to be known for all E and θ. For simplicity, I have chosen to use the same technique I use later on to calculate j. I have found this technique to be useful in minimizing the number of assumptions required and in specifying precisely those that are made. It is a matrix inverse technique that is described in detail by Tarantola and Valette (Reviews of Geophysics and Space Physics, 20, 219-232, 1982). Essentially it provides a least squares solution of eqs. (2) and (4) for R_{ik}. The resulting smoothed response function is

$$\hat{R}(x) = \sum_{m,n} C_0(x,x_m)(\mathrm{S}^{-1})_{mn} R(x_n) \quad (6)$$

where

$$S_{mn} = \sigma_m^2 \delta_{mn} + C_0(x_m,x_n) \quad (7)$$

Here the notation is simplified by dropping the subscripts on R and replacing the pair of variables $(\ln E, \theta)$ by x (E was replaced by its logarithm to give more equal spacing of the data points). $R(x_n)$ is the value obtained from eq. (5) with a standard deviation of σ_n, and S is a $N \times N$ matrix given by eq. (7) with N equal to the number of data points (calibration runs). All of the smoothing information is contained in the function $C_0(x,x')$, which is the expected (prior) covariance between the points x and x'. I have used a Gaussian

$$C_0(x,x') = \sigma^2 \exp\left[-\frac{(\ln E - \ln E')^2}{2\Delta_E^2} - \frac{(\theta-\theta')^2}{2\Delta_\theta^2}\right] \quad (8)$$

where $\sigma \approx 10\text{cm}^2$, $\Delta_E \approx 0.4$ (E in MeV), and $\Delta_\theta \approx 15°$ are constants determined by the expected magnitude of R (σ), and the expected smoothness of R in E (Δ_E) and θ (Δ_θ). Using eq. (6) $\hat{R}$ can be evaluated at any E and θ along with its standard deviation given by $\hat{C}^{1/2}(x,x)$, where $\hat{C}(x,x')$ is the final covariance function (as constrained by the data),

$$\hat{C}(x,x') = C_0(x,x') - \sum_{m,n} C_0(x,x_m)(\mathrm{S}^{-1})_{mn} C_0(x_n,x') \quad (9)$$

Although eq. (6) could be used directly I found it more useful to first replace $R(x_n)$ by its logarithm in order to eliminate the possibility of negative values of R (the square root of R would be another way to do this). Results in a similar format to Figures 3, 4, and 5 are shown in Figures 6, 7, and 8. Figure 9 shows the same results integrated over solid-angle to give the geometry factors at each energy for an isotropic distribution. The integration was done by the trapezoidal rule. Tables of the response functions and geometry factors are available for input to data analysis programs. The tables for P1, ELO, and EHI are shown in Figure 10. Similar tables contain the statistical uncertainties for each response function from eq. (9), but these should be used with caution because systematic errors are not included.

To calculate energy spectra, new event-type channels were defined as follows. First the energy deposit in each detector as measured by Macsys was converted to the corresponding PET ADC channel number using the equations defined in SRL internal report #105 (also in the PET user's document). Only events with energies above the required ADC thresholds were included. The ADC channels for zero energy (given by the integer ratio -B/A of the linear channel-to-energy parameters defined in internal report #105) where then subtracted and the resulting numbers summed according to P1+P2 for ELO events, P1+P2+2·P3 for EHI events, and P1+P2+2·(P3+P47) for range events. Since the P3 and P47 ADC channels are approximately twice as wide as P1 and P2, the resulting new channel numbers are approximately proportional to total energy (~0.15 MeV/channel). To improve statistics, some of these channels were combined to form wider energy intervals. Events that fell into each interval were collected to form response functions that were again calculated with eq. (6). The results are stored as tables in files with the same format as Figure 10. The integrated geometry factors for the useful channels (those with a substantial electron response) are shown in Figures 11, 12, and 13. Response functions for RNG and EWG events have not been calculated in detail because the statistics available from the calibrations at high energies are probably insufficient. In these cases it may be possible to supplement the calibration data with Monte Carlo simulations such as those done by Mark Looper with the EGS program.

The response functions from the calibration data can be used in eq. (2) to calculate $j(E)$ from flight electron data. However, there are several problems in organizing the flight data that must be overcome first:

1. Proton contamination must be eliminated. Although protons are supposed to be eliminated by the P1A discriminator, they can contaminate the electron data by chance coincidences, edge effects, etc. I found that this is minimized by excluding data inside $L = 3$ and by making additional cuts on the pulse heights. The cuts I have used are P1+P2 < 50 for ELO events and P2+P3 < 100 for EHI events. These criteria could be improved, but they are not critical in low counting rate periods.

2. Pileup and chance coincidences. These are significant in high counting rate periods (> a few thousand s^{-1}). So far I have only looked at data with low counting rates.

3. Averaging period. The livetime equation (4) depends on having a significant number of events and rate counts in the time interval. If one or both are small then there can be large errors in the calculated livetime. It is natural to use the six second interval associated with the rate readout and then add up all those in the period or region of interest. However, if the counting rates are small it may be better to use a longer interval. This is further complicated by the SAMPEX orbit that moves rapidly through different spatial regions where the spectra may differ, and also by possible time variations during any averaging period. The choice of strategy can also depend on the PET command state, which was recently changed to accept all events in the ELO counter that trigger P1 only (i.e. P2 and P3 are not considered). Coincidence equations can still be implemented by software, but there will be few of these events compared with the total that trigger P1.

4. P3 and P47 anomalies. These have been described elsewhere.

Once the event data have been selected they are collected into the channels for which corresponding response functions are available, using the method described above for the calibration data. For each averaging interval they are divided by the livetime using eq. (1). As a first example, I have chosen to select events from the L shell range 6 to 7 and used an averaging interval of 6 s. The resulting data from all such intervals during one day are then summed and divided by the number of intervals in the sum to give average, livetime corrected counting rates for each channel. The entire 6 s interval must be within the L shell range to be included in the sum. These final averages can then be compared with the rates predicted by dividing eq. (2) by τ_k, given a sample spectrum $j(E)$.

The simplest way to find $j(E)$ is to parameterize it and fit the predictions of eq. (2) to the data. I have done this using a power law in energy, $j(E) = AE^{-\gamma}$, and an exponential in energy, $j(E) = Ae^{-E/E_0}$. I chose two data sets as described above, one from 1992 day 190 when PET was in its original command state, and one from 1993 day 271 which was after the command state was changed to accept P1 events. In the 1992 data P1 events are not available, but the P1 rate can be used as a single data point to constrain the low energy part of the spectrum. This day was also chosen as a time when the P3 and P47 ADCs appeared to be working, although I am not using the P47 data since they only contribute to RNG events. The 1993 data does include P1 events at the expense of much lower statistics on the ELO events (for the original definition of ELO). The EHI event statistics are also lower but the EHI rate is affected less because P3 is still required to trigger an EHI rate count, although P2 and the guards are not. The original ELO and EHI logic equations are reinstated by software so that the original response functions can also be used.

The data from 1992 day 190 were best fit using an exponential spectrum with $A = 1800$ (cm^2 s sr MeV)$^{-1}$ and $E_0 = 0.40$ MeV. The parameters are from an unweighted non-linear least-squares fit to the logarithm of the counting rate in each channel. Fitting the logarithm is equivalent to giving the data points equal relative uncertainties. The statistical errors were not used because systematic errors in the response functions are probably more important. Data from the ELO and EHI channels used in the fit, along with the simulation due to the exponential spectrum, are shown in Figure 14. The average P1 counting rate of 2400 s^{-1} was also included and the fit predicted 2438 s^{-1}.

A power law fit to the P1 event data from 1993 day 271 is shown in Figure 15. ELO and EHI data were not included in this fit because of poor statistics, but the predictions of the power law model are shown in the figure. Also, the P3 ADC was probably malfunctioning at this time, which would invalidate the EHI data. The best fit parameters were $A = 19$ (cm^2 s sr MeV)$^{-1}$ and $\gamma = 5.2$ These apply to the limited energy range of P1.

The electron spectrum $j(E)$ can also be found by directly solving eq. (2). This can be done by treating j as a continuous function of E as was done for R in eq. (6). However, it is simpler to assume that j is defined at only a discrete set of energies so that eq. (2) becomes a matrix equation

$$d = \mathbf{R} j \qquad (10)$$

where d is a vector containing the counting rates (N_{ik}/τ_k) for each channel, $\mathbf{R}$ is a matrix containing the response functions for each channel evaluated at the spectral energies, and j is the vector forming the discrete spectrum. With notation similar to eq. (6) a solution is

$$\hat{j} = j_0 + \hat{\mathbf{C}} \cdot \mathbf{R}^T \cdot \mathbf{C}_d^{-1} \cdot (d - \mathbf{R} j_0) \qquad (11)$$

where

$$\hat{\mathbf{C}} = (\mathbf{R}^T \cdot \mathbf{C}_d^{-1} \cdot \mathbf{R} + \mathbf{C}_0^{-1})^{-1} \qquad (12)$$

is the covariance matrix of the solution, $\mathbf{C}_d$ is the covariance matrix of the data, which is diagonal since the errors in the data are uncorrelated, and $\mathbf{C}_0$ is the prior covariance matrix. The vector j_0 is an initial guess at the spectrum and $\mathbf{C}_0$ represents the degree of confidence in this guess. It is still useful to include some smoothing, since fluctuations in the data tend to be amplified by the matrix inverse, so I have again used a Gaussian in energy similar to eq. (8). I found that the best power law fit to the data was a good choice for j_0. The spectrum resulting from the 1992 day 190 data is shown in Figure 16, along with j_0 for comparison. The EHI data were not included in the fit. To compensate for systematic effects the error bars on the data, which go into $\mathbf{C}_d$, were assumed to be 10% instead of the statistical errors. The error bars on $\hat{j}$ result from eq. (12) and in regions where they are small the data is constraining the model. Note that the P1 rate provides a constraint near its threshold energy of ~0.5-0.6 MeV, but then there is a gap until the ELO event data become important from ~1.5 to ~3.5

MeV. The fit to the ELO data resulting from the model spectrum in Figure 16 is shown in Figure 17. The P1 rate predicted by the model was 2388 s^{-1}, compared to 2400 s^{-1} from the data.

Some aspects of the data analysis that should be improved or further considered are: the effects of pileup and chance coincidences in high counting rate regions; the validity of the deadtime corrections and averaging periods; the importance of anisotropic electron distributions for which the full angular response functions and spacecraft pointing information would need to be incorporated; and the error analysis of the response functions, event data, and energy spectra.

Figure Captions

1. Beam profile and contour map from the β-spectrometer calibration. The location of PET is shown by the X. The contours are spaced every 0.5 $(cm^2s)^{-1}$ and range from 0.5 to 6.0 $(cm^2s)^{-1}$. Note that the beam was not fully mapped around the edges.

2. Response function (effective area) for P1 singles events from eq. (5). The β-spectrometer data are on the left and the accelerator data on the right. The points for each angle are connected. Satistical error bars are included.

3. Similar to Figure 2 but corrected for accelerator beam divergence. The β-spectrometer data are unchanged.

4. Similar to Figure 3 but for ELO events.

5. Similar to Figure 3 but for EHI events.

6. Smoothed P1 singles response function from eq. (6). The points are at approximately twice the energy resolution of the calibration runs and every 10° in θ.

7. Similar to Figure 6 but for ELO events.

8. Similar to Figure 6 but for EHI events.

9. P1, ELO, and EHI geometry factors versus energy for isotropic electron distributions.

10. Tables of the P1 (a), ELO (b), and EHI (c) response functions. The first column on the left column is the energy in MeV, the second column is the geometry factor shown in figure 9, the remaining columns are the response function values shown in Figure 7 with the angle in degrees at the top.

11. P1 geometry factors versus energy for the individual channels described in the text. When two or more channels are summed to form a single response function the following convention is used for the labels on each plot and for the file names containing the response functions: the channel numbers before the decimal point refer to the lowest channel included, the number after the decimal point is the number of channels included in the sum. For example, 006.2 includes channels 6 and 7.

12. (a),(b) Similar to Figure 11 but for ELO.

13. Similar to Figure 11 but for EHI.

14. ELO and EHI event data from 1992 day 190 (histograms), and the model simulation based on the exponential fit described in the text (data points with error bars based on the calibration statistics). The e-folding energy is $E_0 = 0.40$ MeV.

15. P1 event data with a power-law fit from 1993 day 271, in a similar format to Figure 14. ELO and EHI data were not included in the fit. The spectral index is $\gamma = 5.2$.

16. Electron energy spectra for 1992 day 190 derived from a power-law fit (dashed line, $\gamma = 3$) and eq.

(11) (histogram with error bars), as described in the text.

17. Simulated ELO data from the spectrum in Figure 16, in the same format as Figure 14. The P1 counting rate was included in the fit but not the EHI data.

Figure 1

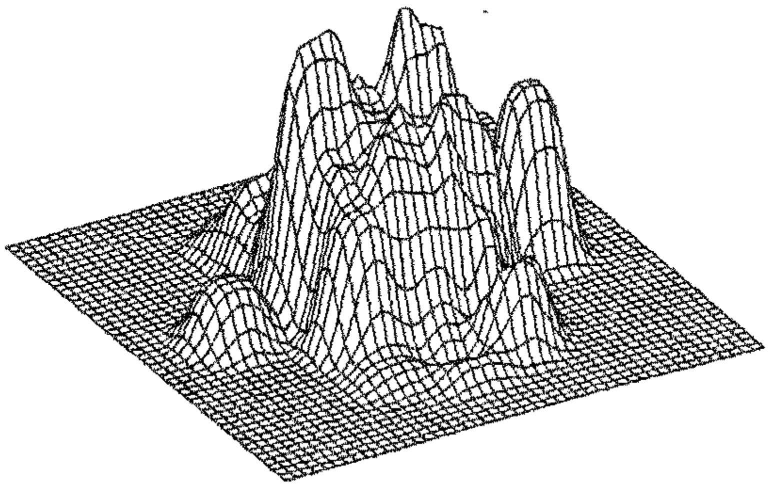

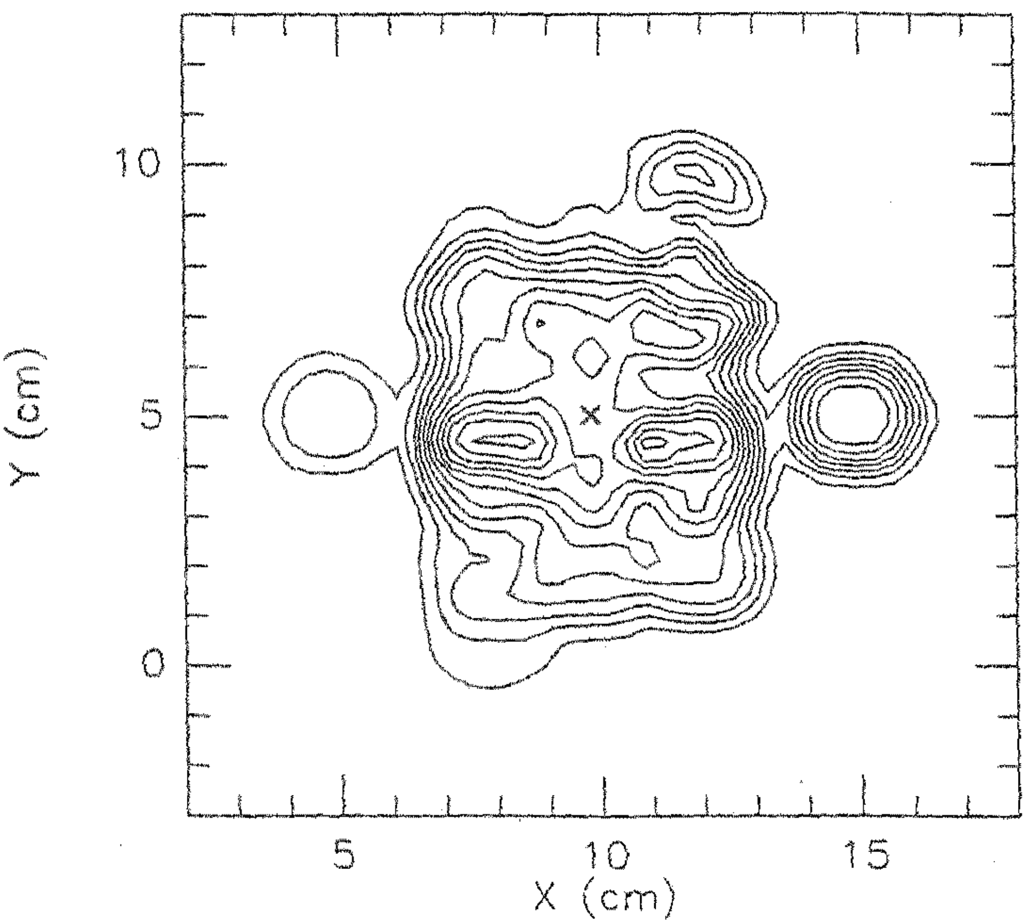

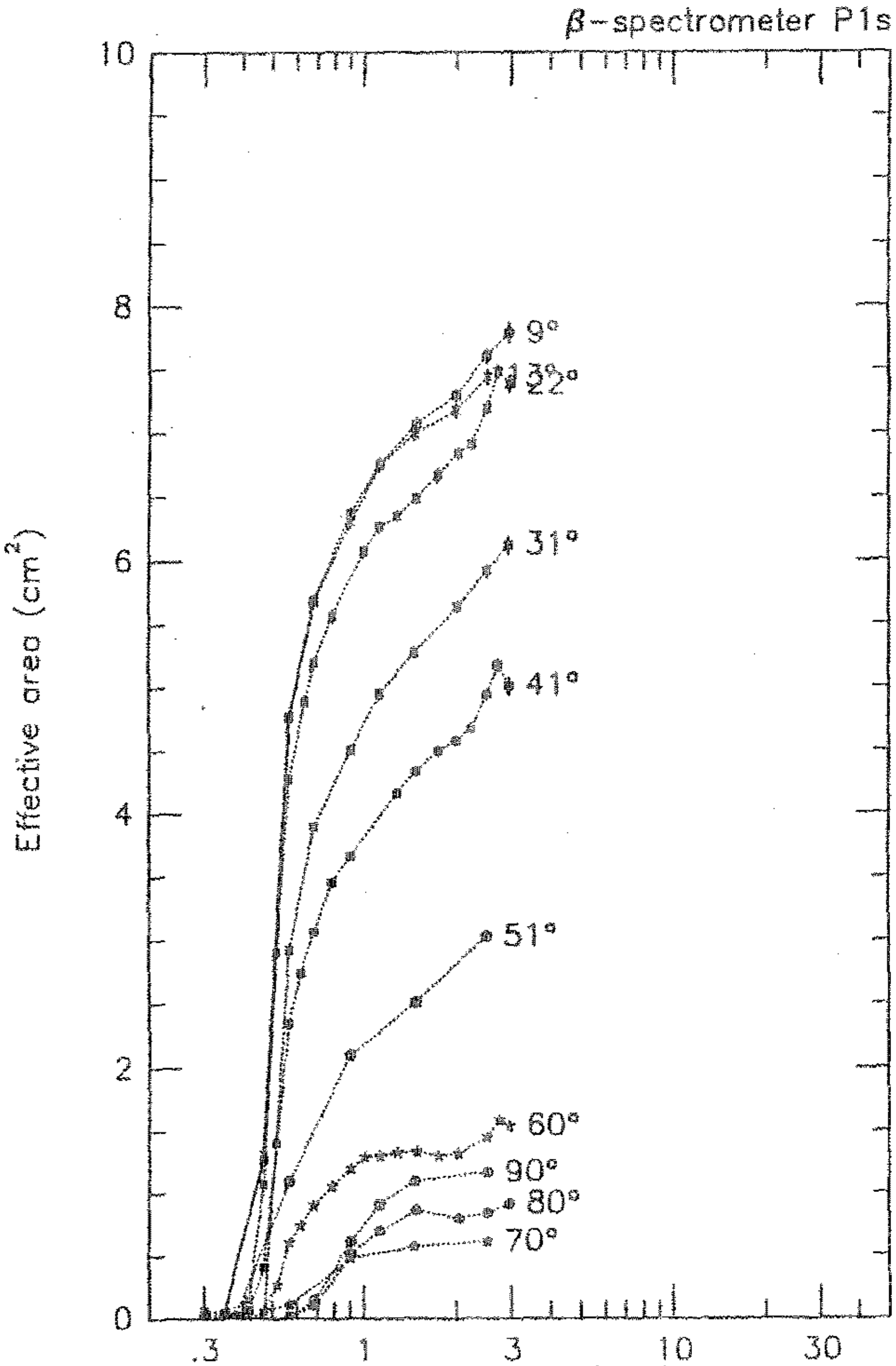
β-spectrometer P1s
Effective area (cm²)
10
8
6
4
2
0
.3
1
3
10
30
9°
31°
41°
51°
60°
90°
80°
70°

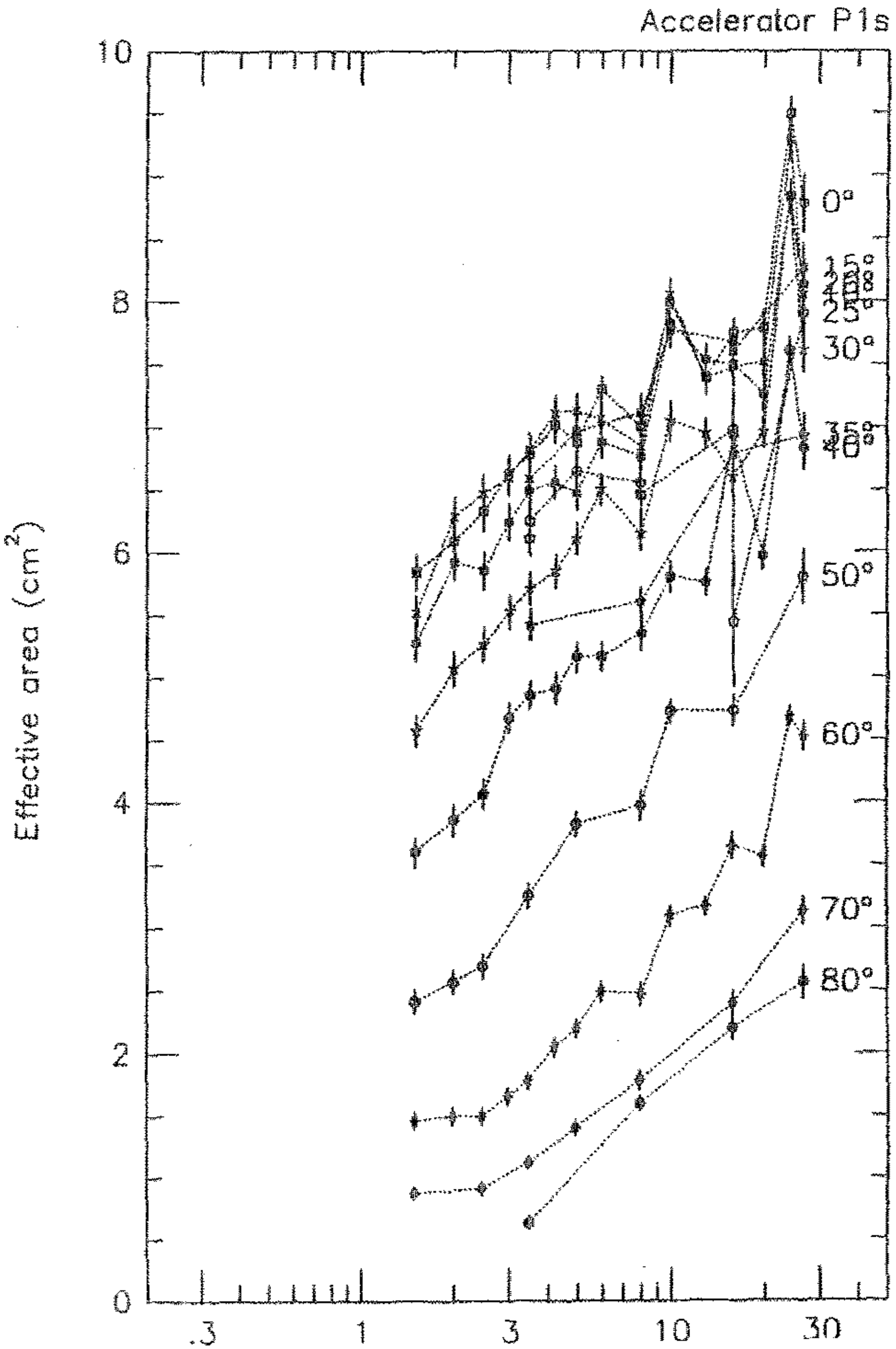
Accelerator P1s
Effective area (cm²)
10
8
6
4
2
0
.3
1
3
10
30
0°
30°
50°
60°
70°
80°

Figure 2

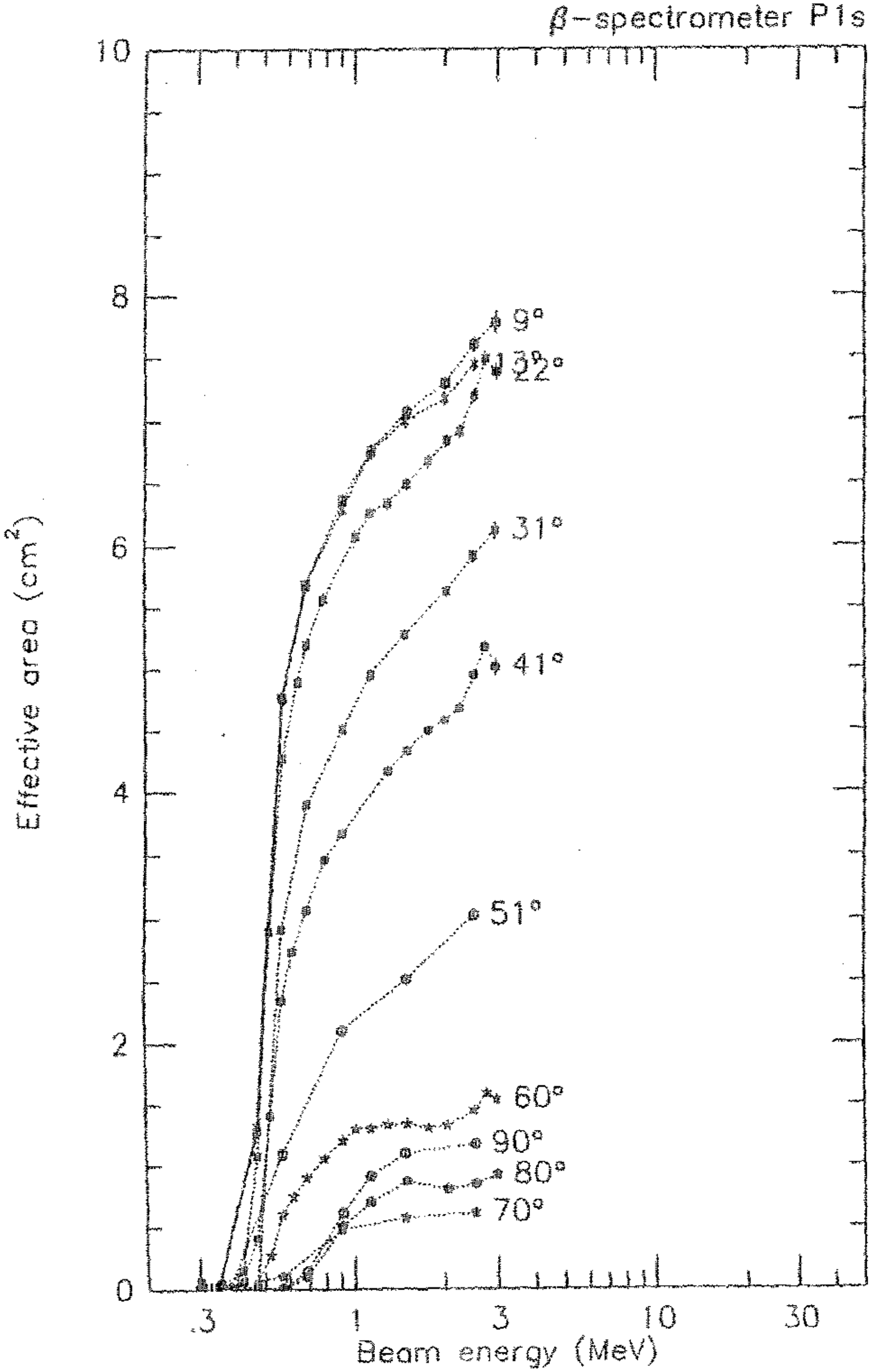
β-spectrometer P1s
Effective area (cm²)
Beam energy (MeV)
9°
13°
22°
31°
41°
51°
60°
90°
80°
70°

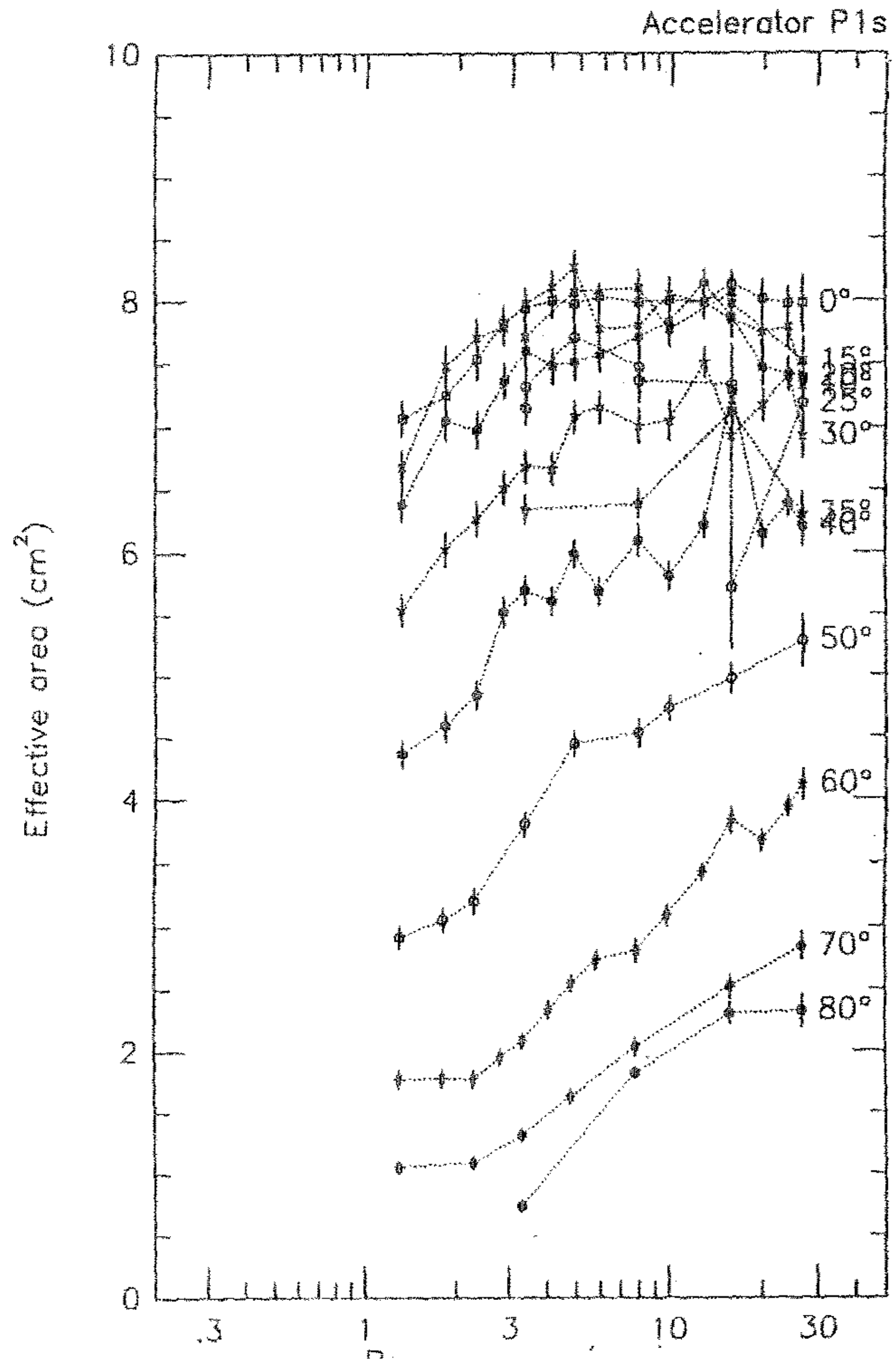
Accelerator P1s
Effective area (cm²)
0°
15°
25°
30°
40°
50°
60°
70°
80°

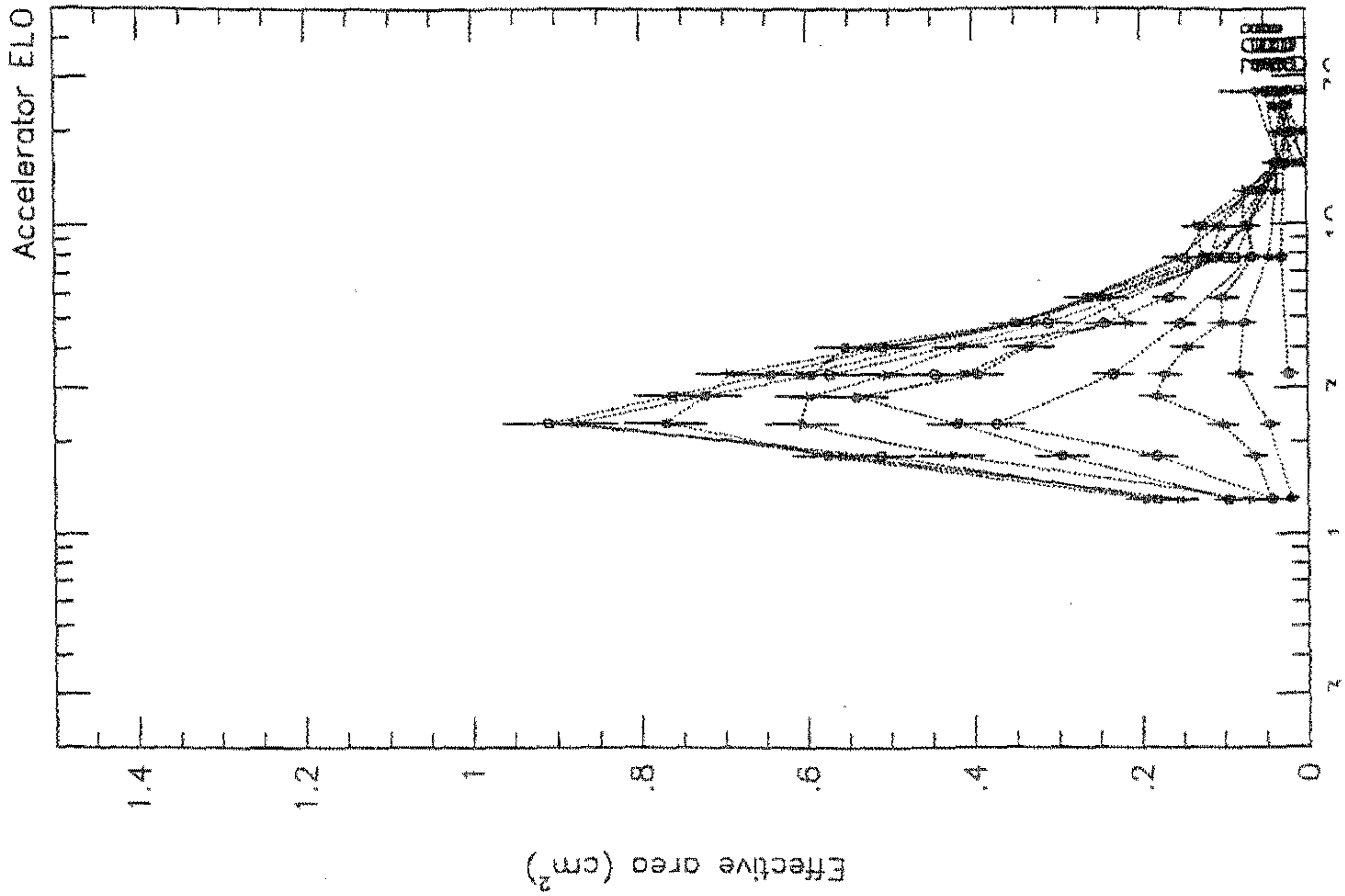
Accelerator ELO
Effective area (cm²)
1.4
1.2
1
.8
.6
.4
.2
0

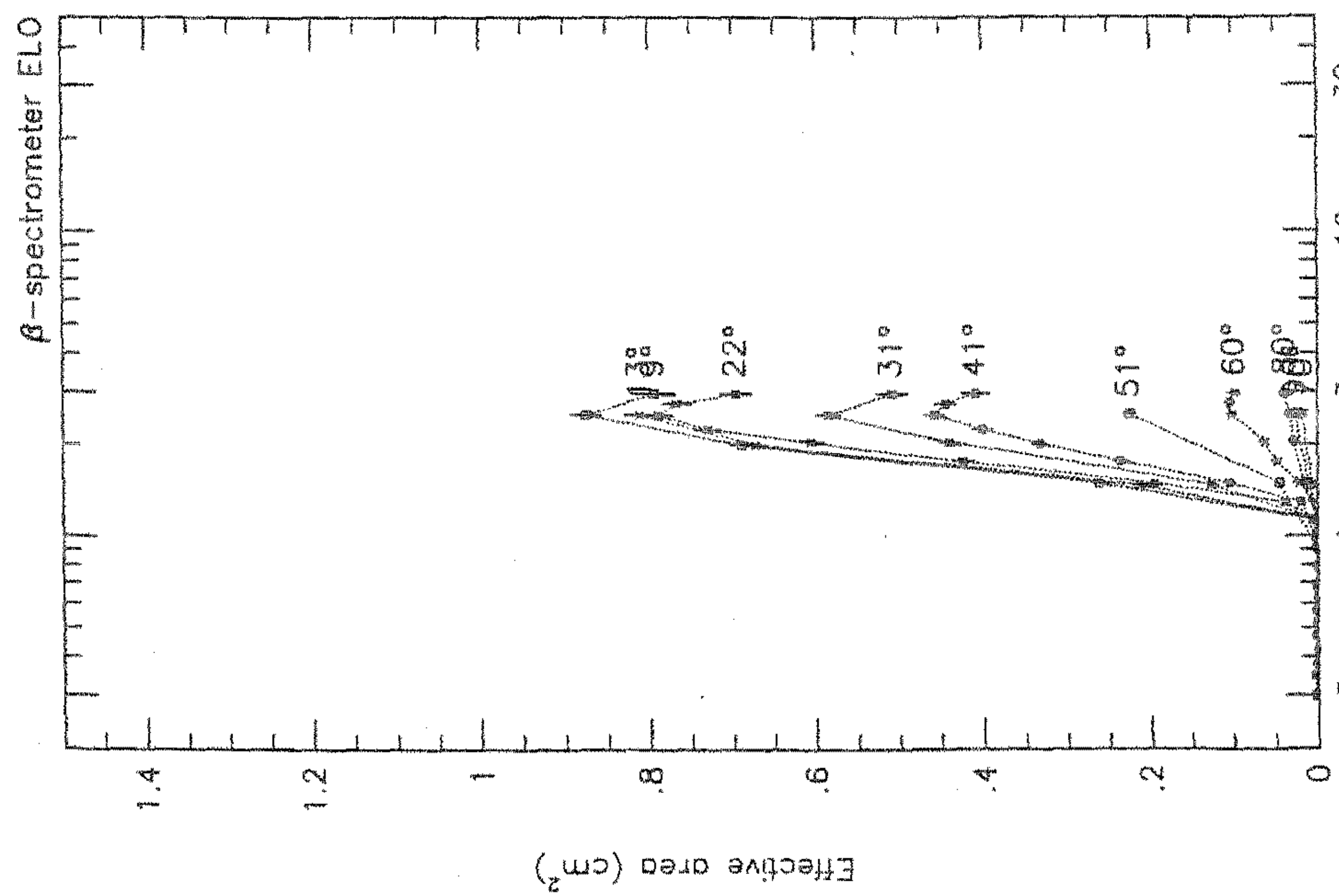
β-spectrometer ELO
Effective area (cm²)
1.4
1.2
1
.8
.6
.4
.2
0
22°
31°
41°
51°
60°
.3
1
3
10

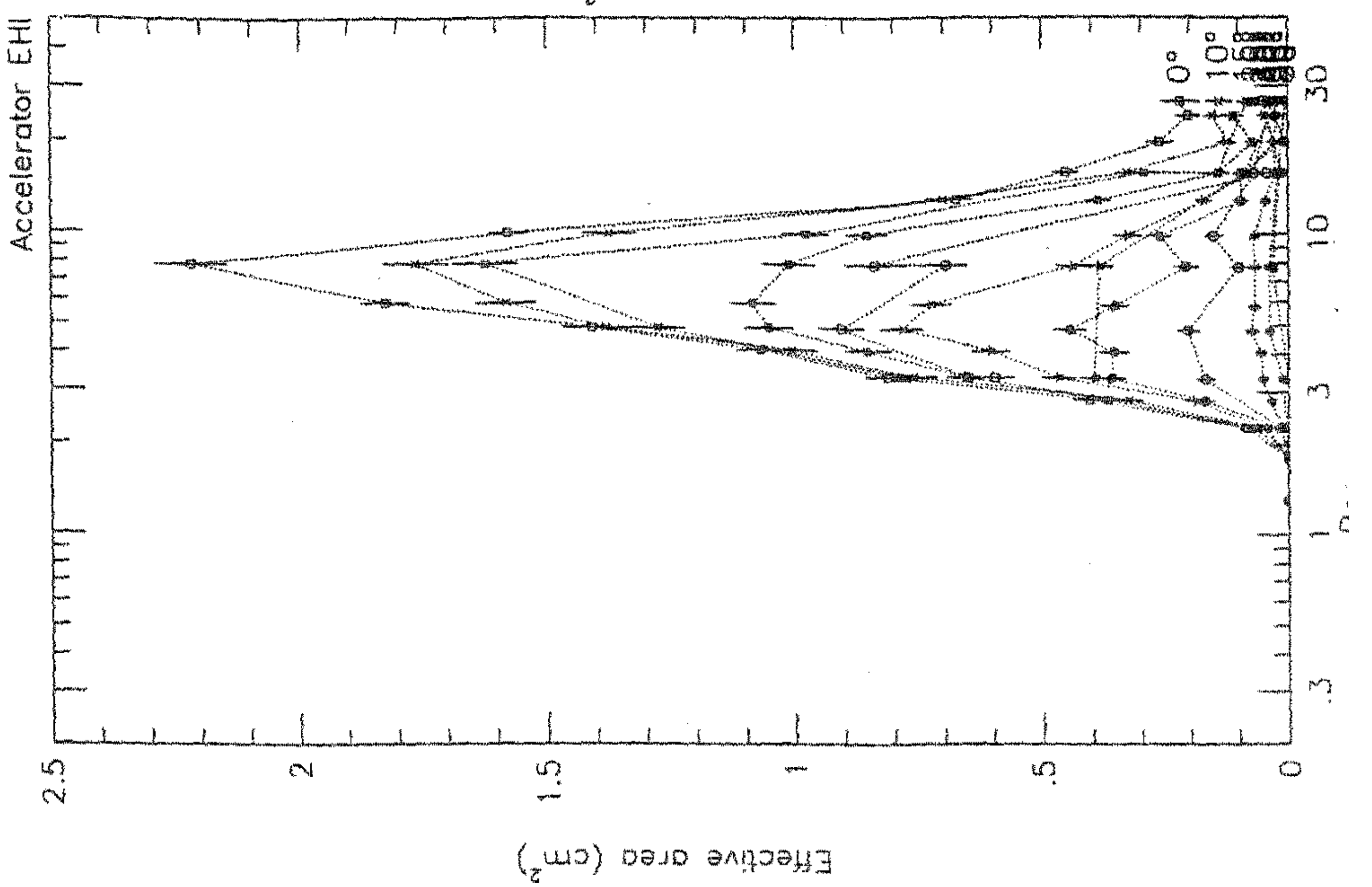
Accelerator EHI
Effective area (cm²)
2.5
2
1.5
1
.5
0
.3
1
3
10
30
0°
10°

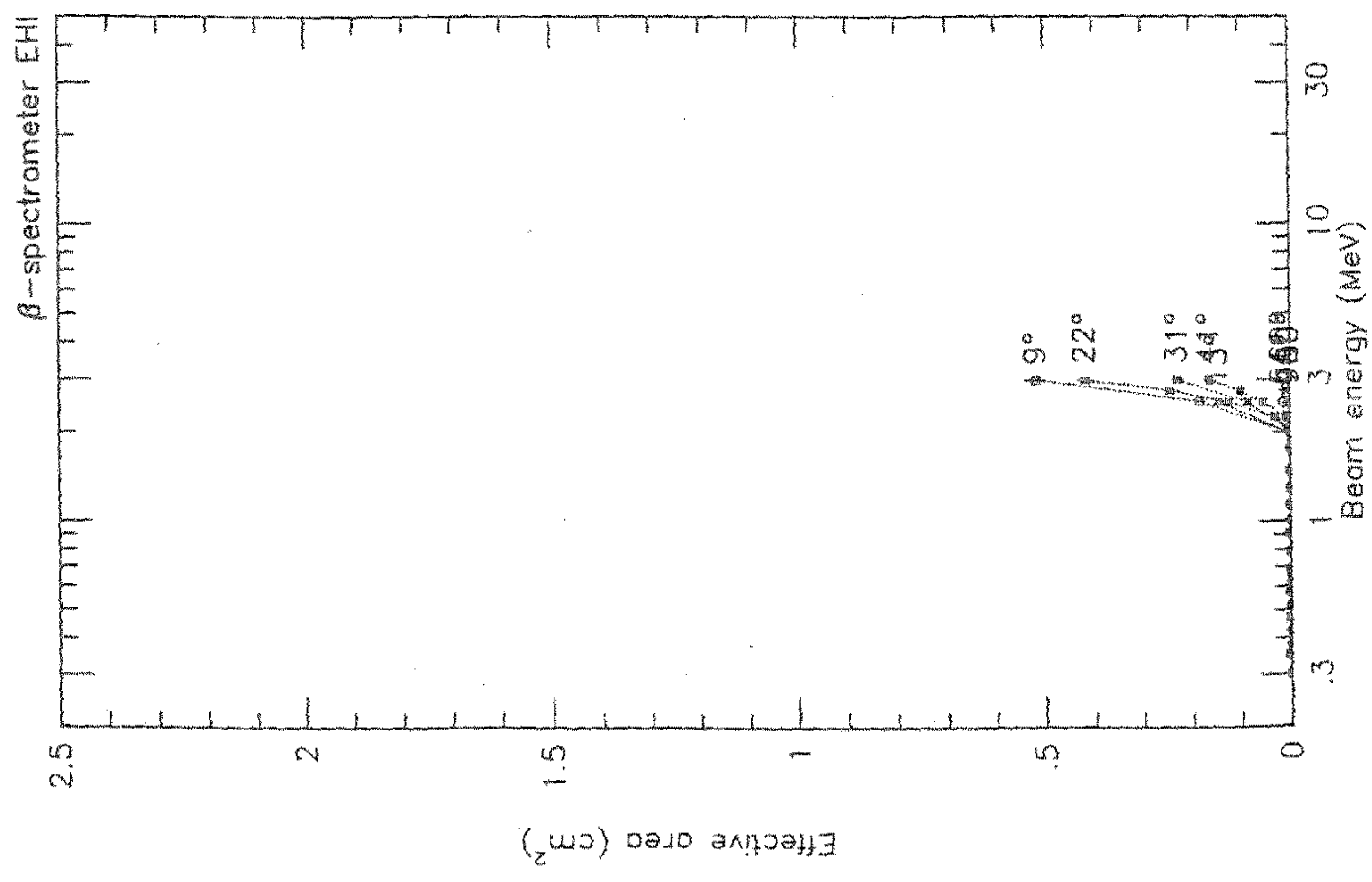
β-spectrometer EHI
Effective area (cm²)
Beam energy (MeV)
2.5
2
1.5
1
.5
0
.3
1
3
10
30
9°
22°
31°

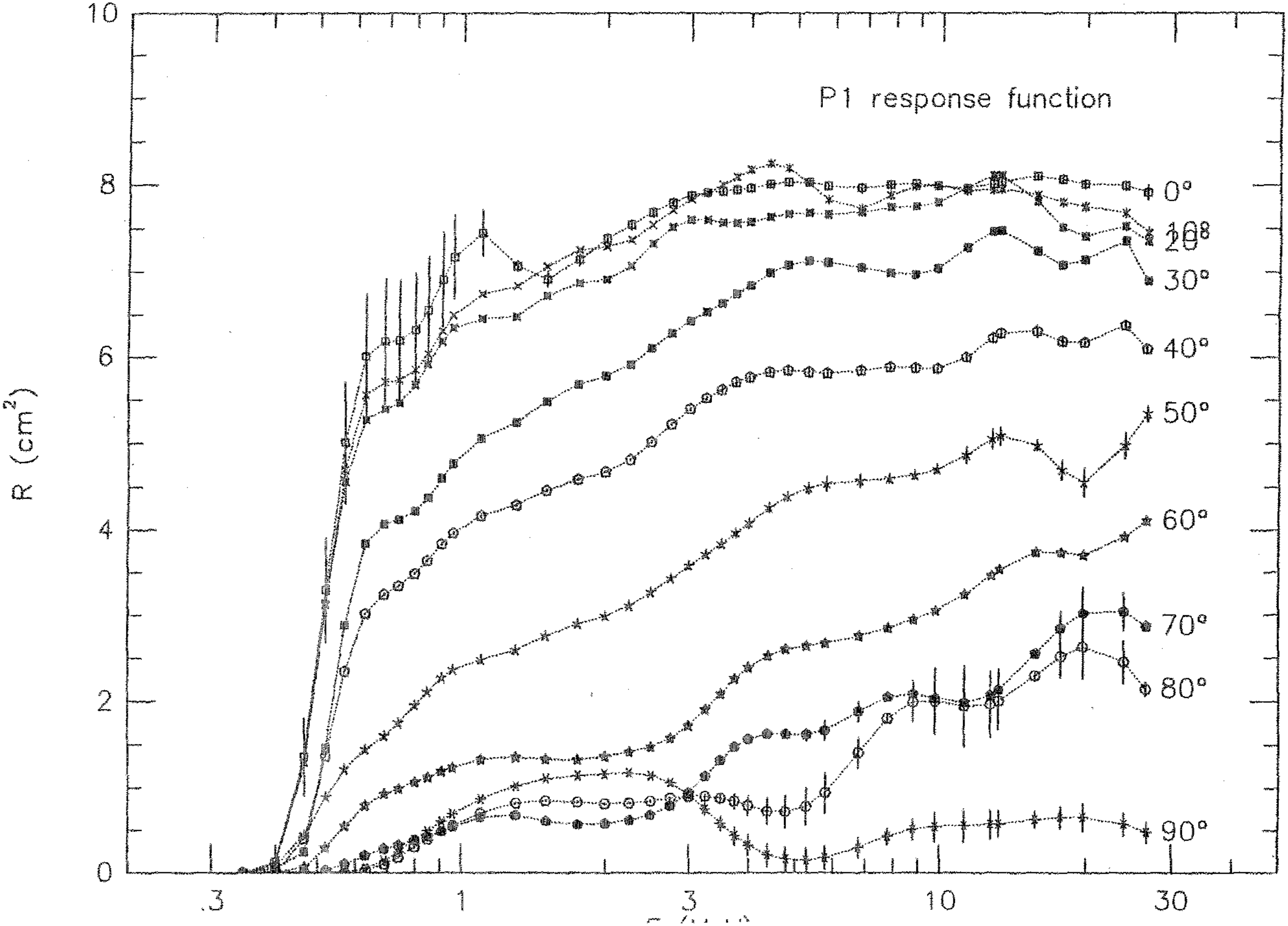
P1 response function
R (cm²)
0°
10°
20°
30°
40°
50°
60°
70°
80°
90°
.3
1
3
10
30
0
2
4
6
8
10

Figure 6

07/27/2006 THU 08:05 FAX 310 336 1636 AEROSPACE

Figure 7

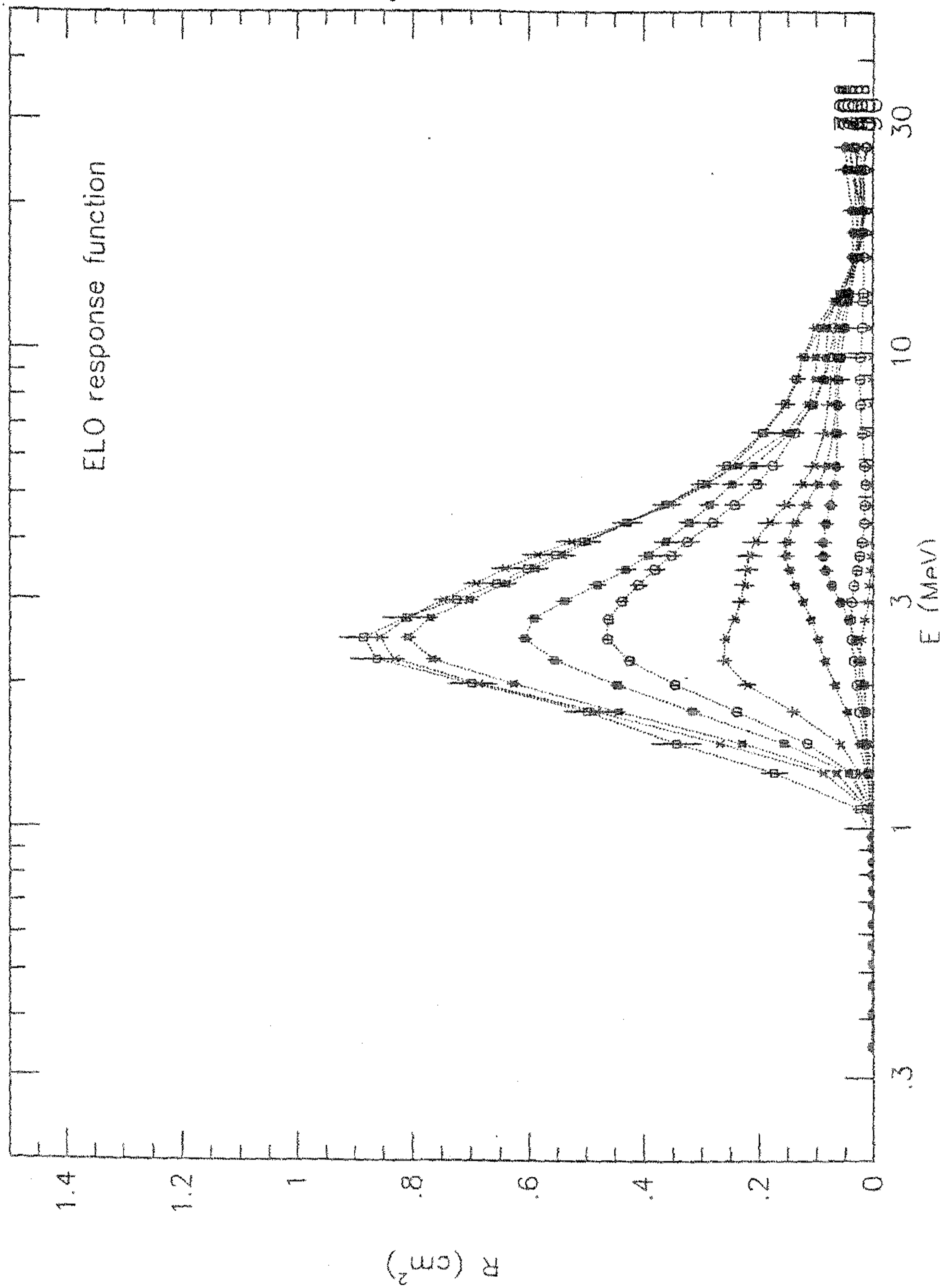

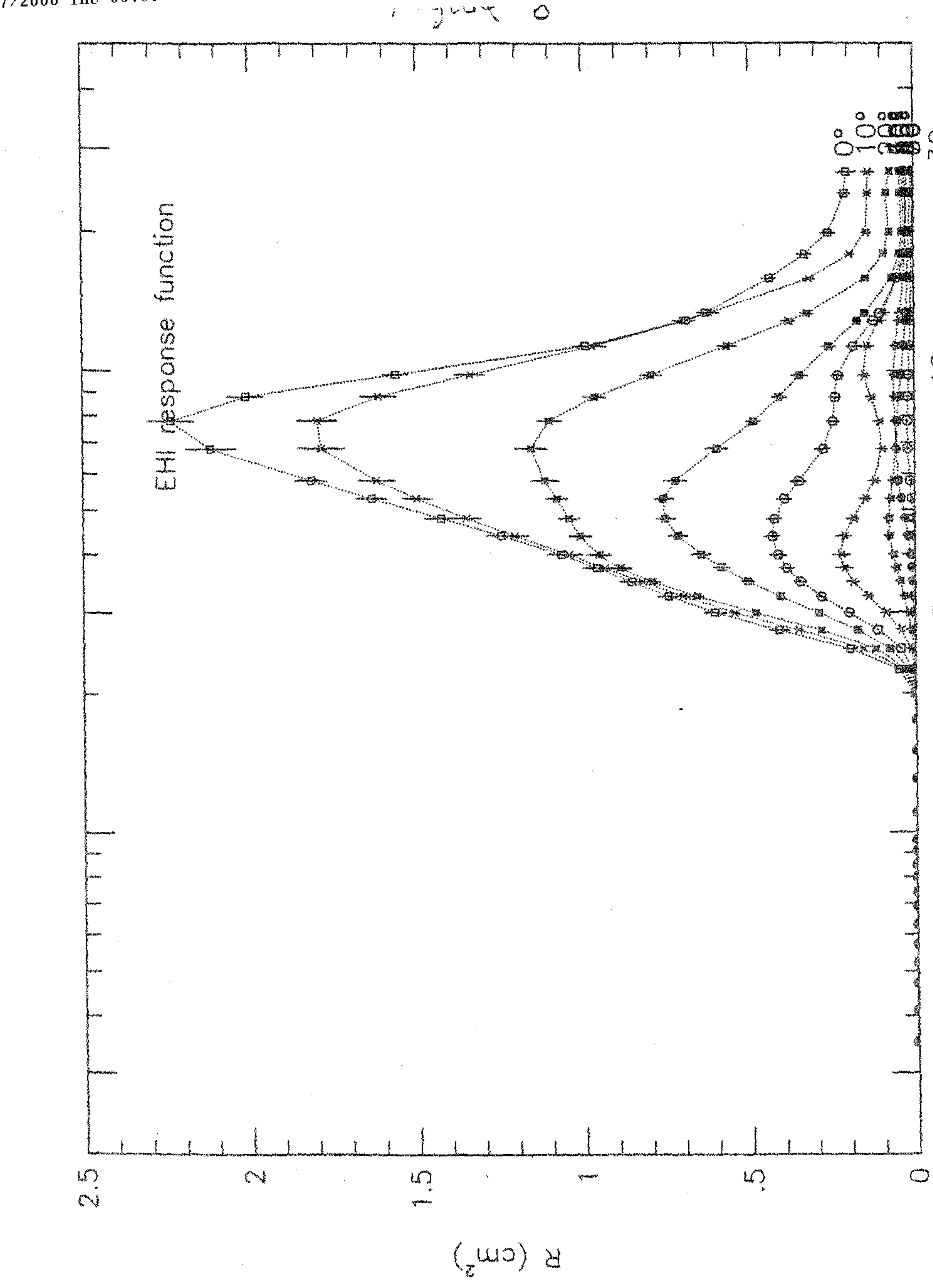
EHI response function
R (cm²)
2.5
2
1.5
1
.5
0
3
1
3
10
0°
10°

Figure 9

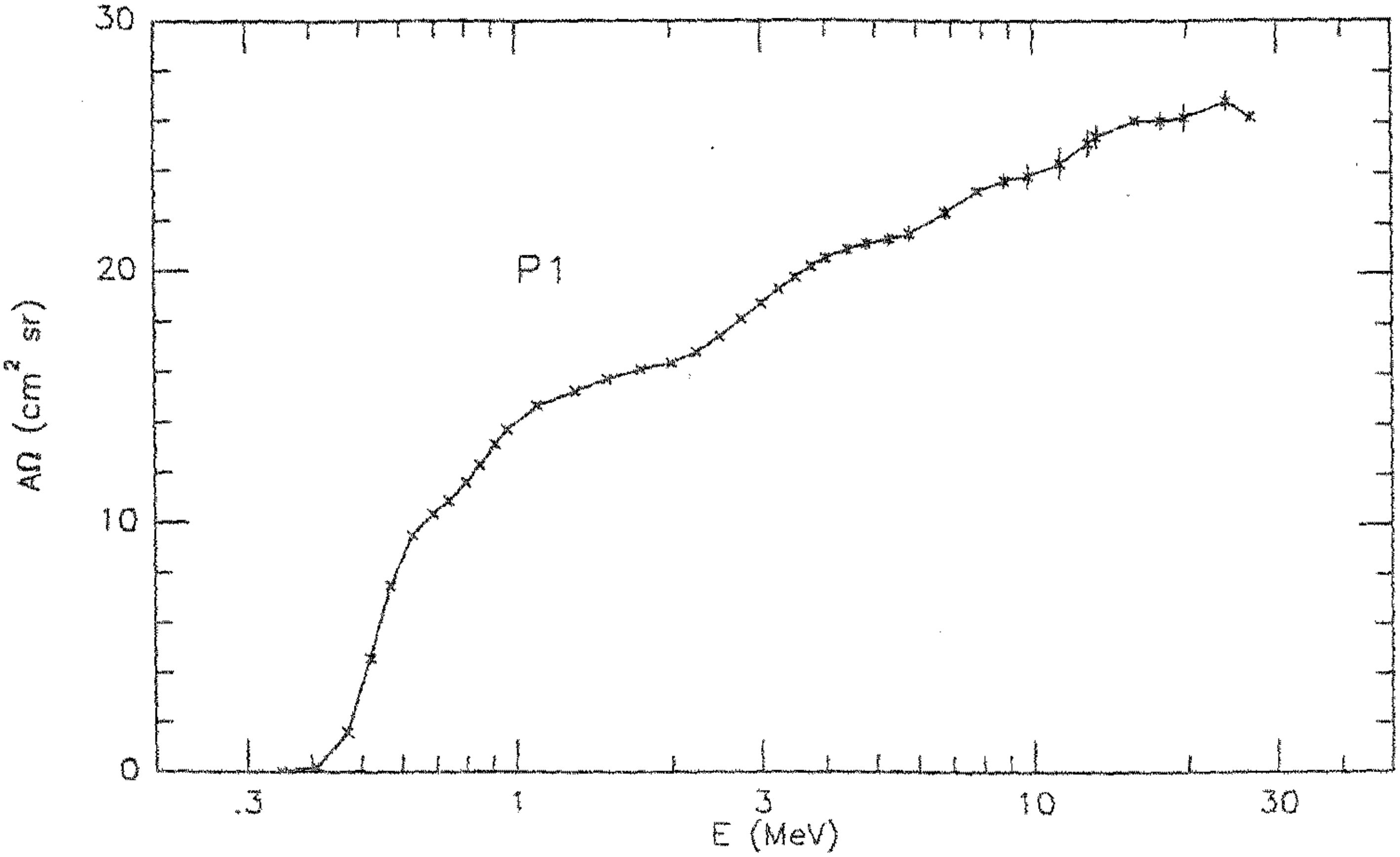
30
20
10
0
AΩ (cm² sr)
P1
.3
1
3
10
30
E (MeV)

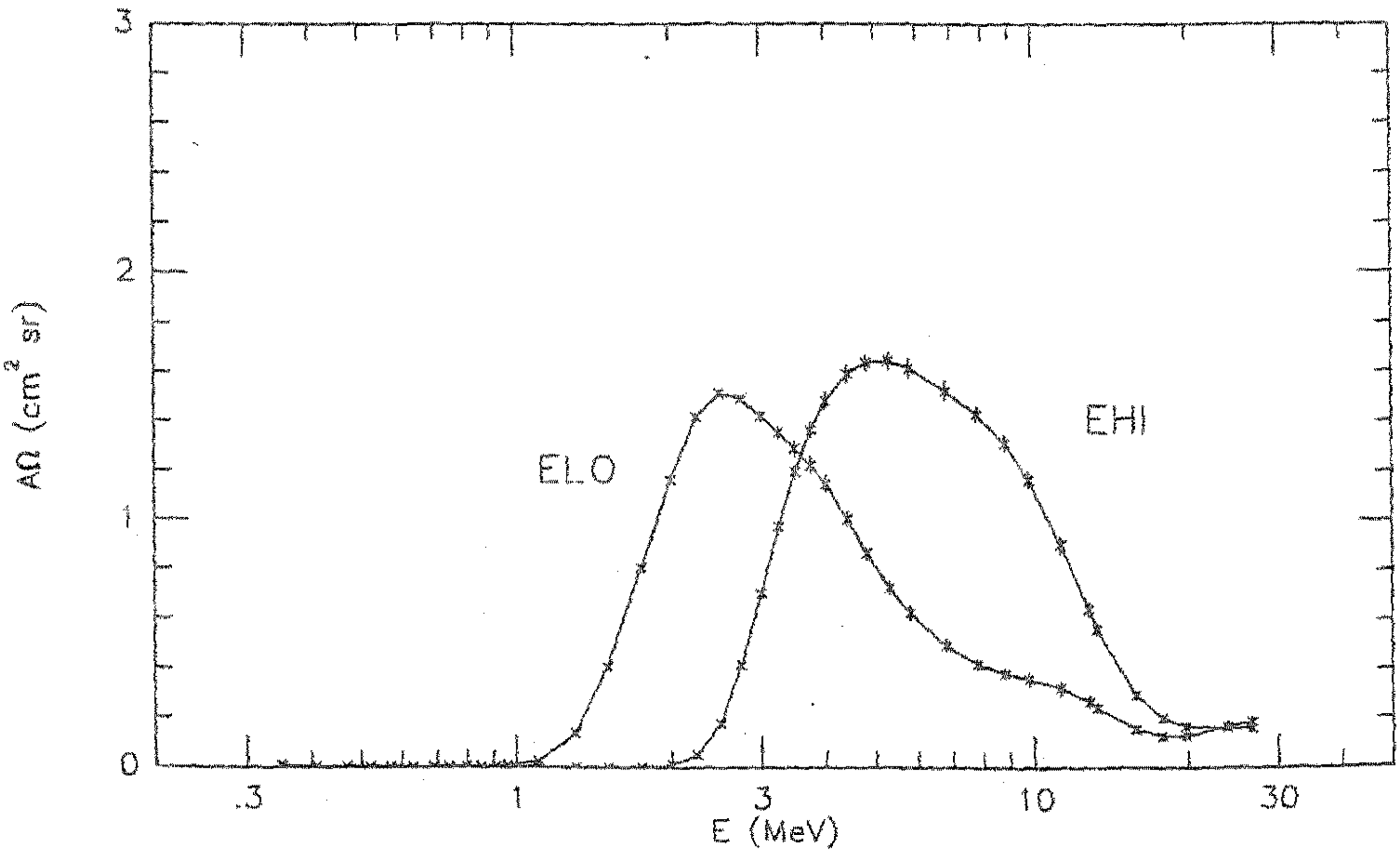
3
2
1
0
AΩ (cm² sr)
ELO
EHI
.3
1
3
10
30
E (MeV)

home/skrymir2/sampex/rss/petcal/smrespS.pls Wed Oct 13 10:03:04 1993 1

Figure 10(a)

		0.000	10.000	20.000	30.000	40.000	50.000	60.000	70.000	80.000	90.000
0.350	0.013	0.000	0.000	0.000	0.012	0.002	0.001	0.003	0.002	0.000	0.000
0.410	0.183	0.135	0.114	0.107	0.053	0.001	0.074	0.002	0.021	0.005	0.000
0.470	1.599	1.361	1.290	1.302	0.245	0.398	0.448	0.068	0.000	0.009	0.000
0.520	4.575	3.292	3.132	3.118	1.461	1.363	0.882	0.290	0.028	0.003	0.001
0.570	7.503	5.009	4.702	4.562	2.886	2.349	1.214	0.553	0.104	0.001	0.010
0.630	9.496	6.008	5.560	5.271	3.836	3.014	1.444	0.788	0.202	0.030	0.053
0.690	10.335	6.192	5.712	5.396	4.076	3.244	1.607	0.924	0.277	0.102	0.143
0.740	10.847	6.197	5.727	5.465	4.119	3.342	1.755	0.997	0.325	0.186	0.247
0.800	11.588	6.323	5.849	5.672	4.222	3.486	1.952	1.067	0.377	0.299	0.384
0.850	12.309	6.558	6.044	5.914	4.379	3.641	2.113	1.124	0.424	0.390	0.494
0.910	13.148	6.910	6.307	6.186	4.605	3.832	2.272	1.189	0.486	0.488	0.612
0.960	13.728	7.175	6.495	6.345	4.774	3.964	2.364	1.237	0.538	0.558	0.694
1.100	14.674	7.447	6.737	6.455	5.050	4.163	2.484	1.331	0.656	0.707	0.867
1.300	15.249	7.073	6.832	6.486	5.241	4.294	2.596	1.356	0.677	0.821	1.025
1.500	15.751	6.918	7.067	6.722	5.485	4.463	2.757	1.330	0.609	0.848	1.109
1.750	16.116	7.146	7.256	6.872	5.684	4.596	2.895	1.327	0.566	0.829	1.147
2.000	16.372	7.386	7.287	6.911	5.778	4.676	2.987	1.366	0.584	0.815	1.167
2.250	16.827	7.547	7.373	7.075	5.914	4.817	3.109	1.415	0.623	0.823	1.178
2.500	17.466	7.684	7.541	7.328	6.103	5.018	3.265	1.479	0.684	0.847	1.150
2.750	18.137	7.801	7.708	7.523	6.284	5.223	3.425	1.579	0.790	0.877	1.062
3.000	18.761	7.879	7.829	7.602	6.427	5.394	3.573	1.726	0.948	0.898	0.920
3.250	19.319	7.917	7.918	7.600	6.538	5.527	3.709	1.905	1.137	0.900	0.751
3.500	19.813	7.933	8.004	7.573	6.639	5.628	3.837	2.090	1.323	0.879	0.583
3.750	20.235	7.948	8.095	7.563	6.741	5.708	3.962	2.256	1.473	0.840	0.440
4.000	20.573	7.969	8.179	7.579	6.844	5.770	4.082	2.389	1.571	0.793	0.328
4.400	20.942	8.009	8.249	7.630	6.990	5.831	4.256	2.530	1.630	0.733	0.215
4.800	21.148	8.035	8.202	7.670	7.085	5.848	4.390	2.603	1.626	0.719	0.163
5.300	21.326	8.029	8.023	7.677	7.126	5.832	4.494	2.648	1.626	0.788	0.153
5.800	21.576	7.997	7.834	7.665	7.114	5.817	4.543	2.680	1.675	0.945	0.181
6.800	22.435	7.968	7.726	7.691	7.055	5.849	4.576	2.756	1.882	1.409	0.302
7.800	23.276	8.005	7.879	7.741	6.997	5.892	4.605	2.850	2.053	1.812	0.430
8.800	23.687	8.021	7.991	7.757	6.973	5.878	4.644	2.947	2.091	1.994	0.512
9.800	23.866	7.995	7.990	7.798	7.040	5.871	4.707	3.050	2.042	2.006	0.546
1.300	24.361	7.969	7.943	7.974	7.287	6.005	4.876	3.241	1.988	1.945	0.559
2.800	25.169	8.017	7.946	8.117	7.473	6.229	5.059	3.465	2.076	1.971	0.573
3.300	25.422	8.041	7.950	8.120	7.485	6.287	5.096	3.536	2.138	2.006	0.581
5.800	26.053	8.109	7.895	7.814	7.248	6.310	4.981	3.743	2.554	2.298	0.630
7.800	26.065	8.071	7.804	7.516	7.081	6.187	4.701	3.734	2.848	2.523	0.658
9.800	26.198	8.018	7.751	7.416	7.148	6.180	4.558	3.707	3.019	2.633	0.659
4.000	26.833	8.000	7.684	7.530	7.364	6.379	4.983	3.921	3.041	2.457	0.574
5.700	26.197	7.915	7.452	7.355	6.894	6.099	5.345	4.109	2.875	2.148	0.483

/home/skrymir2/sampex/rss/petcal/smrespL.elo Wed Oct 13 09:43:24 1993 1

		0.000	10.000	20.000	30.000	40.000	50.000	60.000	70.000	80.000	90.000
0.350	0.006	0.001	0.003	0.002	0.001	0.001	0.001	0.001	0.000	0.000	0.000
0.410	0.004	0.001	0.002	0.002	0.001	0.001	0.001	0.001	0.000	0.000	0.000
0.470	0.004	0.001	0.002	0.002	0.001	0.000	0.001	0.001	0.000	0.000	0.000
0.520	0.003	0.000	0.001	0.002	0.001	0.000	0.000	0.001	0.000	0.000	0.000
0.570	0.003	0.000	0.001	0.002	0.001	0.000	0.000	0.000	0.000	0.000	0.000
0.630	0.002	0.000	0.000	0.001	0.001	0.000	0.000	0.000	0.000	0.000	0.000
0.690	0.002	0.000	0.000	0.001	0.000	0.000	0.000	0.000	0.000	0.000	0.000
0.740	0.002	0.000	0.000	0.000	0.000	0.000	0.000	0.001	0.000	0.000	0.000
0.800	0.003	0.000	0.000	0.000	0.000	0.000	0.001	0.001	0.001	0.000	0.000
0.850	0.004	0.000	0.000	0.000	0.000	0.000	0.001	0.001	0.001	0.000	0.000
0.910	0.005	0.001	0.000	0.000	0.000	0.001	0.001	0.001	0.001	0.001	0.000
0.960	0.008	0.002	0.001	0.001	0.001	0.001	0.002	0.002	0.002	0.001	0.000
1.100	0.025	0.024	0.007	0.006	0.004	0.005	0.005	0.004	0.003	0.003	0.001
1.300	0.136	0.173	0.087	0.064	0.042	0.036	0.021	0.011	0.008	0.009	0.004
1.500	0.408	0.343	0.267	0.228	0.156	0.115	0.058	0.024	0.011	0.016	0.009
1.750	0.805	0.497	0.481	0.443	0.315	0.238	0.139	0.045	0.013	0.023	0.017
2.000	1.160	0.698	0.685	0.626	0.445	0.345	0.221	0.067	0.015	0.028	0.022
2.250	1.415	0.861	0.830	0.765	0.554	0.425	0.260	0.084	0.020	0.032	0.023
2.500	1.513	0.884	0.856	0.808	0.607	0.462	0.258	0.096	0.029	0.036	0.020
2.750	1.490	0.811	0.808	0.769	0.591	0.461	0.243	0.108	0.041	0.038	0.014
3.000	1.422	0.724	0.746	0.702	0.538	0.438	0.232	0.122	0.057	0.036	0.009
3.250	1.354	0.656	0.691	0.639	0.480	0.409	0.226	0.137	0.072	0.032	0.006
3.500	1.290	0.602	0.640	0.587	0.431	0.381	0.222	0.148	0.083	0.027	0.004
3.750	1.223	0.553	0.584	0.541	0.392	0.353	0.217	0.153	0.088	0.023	0.003
4.000	1.144	0.504	0.524	0.498	0.362	0.325	0.207	0.152	0.088	0.019	0.002
4.400	1.003	0.428	0.430	0.428	0.321	0.281	0.182	0.138	0.083	0.015	0.001
4.800	0.865	0.362	0.354	0.363	0.286	0.242	0.154	0.118	0.075	0.014	0.001
5.300	0.724	0.300	0.289	0.292	0.246	0.203	0.124	0.097	0.068	0.013	0.001
5.800	0.622	0.256	0.247	0.235	0.209	0.176	0.104	0.082	0.064	0.015	0.001
6.800	0.493	0.194	0.190	0.155	0.145	0.137	0.086	0.069	0.062	0.019	0.001
7.800	0.419	0.155	0.152	0.114	0.104	0.107	0.078	0.065	0.061	0.022	0.001
8.800	0.379	0.135	0.132	0.101	0.086	0.086	0.073	0.064	0.059	0.023	0.002
9.800	0.357	0.121	0.122	0.100	0.082	0.075	0.069	0.062	0.055	0.022	0.001
11.300	0.322	0.093	0.101	0.092	0.080	0.067	0.063	0.056	0.049	0.019	0.001
12.800	0.262	0.062	0.069	0.064	0.065	0.056	0.051	0.045	0.043	0.017	0.001
13.300	0.239	0.053	0.059	0.054	0.058	0.052	0.046	0.041	0.042	0.017	0.001
15.800	0.152	0.030	0.032	0.025	0.029	0.030	0.026	0.025	0.036	0.016	0.001
17.800	0.125	0.026	0.028	0.020	0.021	0.021	0.017	0.019	0.035	0.017	0.001
19.800	0.125	0.026	0.031	0.022	0.021	0.018	0.014	0.018	0.037	0.017	0.001
24.000	0.164	0.020	0.033	0.039	0.035	0.025	0.019	0.026	0.047	0.015	0.001
26.700	0.183	0.011	0.024	0.041	0.043	0.033	0.025	0.034	0.048	0.012	0.001

Figure 10(b)

ome/skrymir2/sampex/rss/petcal/smrespL.ehi Wed Oct 13 09:47:18 1993 1

		0.000	10.000	20.000	30.000	40.000	50.000	60.000	70.000	80.000	90.000
0.350	0.009	0.003	0.004	0.001	0.001	0.001	0.002	0.002	0.001	0.001	0.000
0.410	0.005	0.003	0.003	0.001	0.001	0.001	0.001	0.001	0.001	0.001	0.000
0.470	0.003	0.002	0.002	0.001	0.000	0.000	0.001	0.001	0.001	0.000	0.000
0.520	0.002	0.002	0.001	0.000	0.000	0.000	0.000	0.000	0.000	0.000	0.000
0.570	0.002	0.001	0.001	0.000	0.000	0.000	0.000	0.000	0.000	0.000	0.000
0.630	0.002	0.002	0.001	0.000	0.000	0.000	0.000	0.000	0.000	0.000	0.000
0.690	0.003	0.002	0.002	0.001	0.000	0.000	0.001	0.000	0.000	0.000	0.000
0.740	0.003	0.002	0.002	0.001	0.001	0.001	0.001	0.000	0.000	0.000	0.000
0.800	0.004	0.003	0.003	0.001	0.001	0.001	0.001	0.001	0.000	0.000	0.000
0.850	0.004	0.003	0.004	0.002	0.001	0.001	0.001	0.001	0.000	0.000	0.000
0.910	0.004	0.002	0.003	0.002	0.001	0.001	0.001	0.000	0.000	0.000	0.000
0.960	0.003	0.002	0.002	0.001	0.001	0.001	0.001	0.000	0.000	0.000	0.000
1.100	0.001	0.000	0.001	0.000	0.000	0.000	0.000	0.000	0.000	0.000	0.000
1.300	0.001	0.000	0.000	0.000	0.000	0.000	0.000	0.000	0.000	0.000	0.000
1.500	0.001	0.000	0.000	0.000	0.000	0.000	0.000	0.000	0.000	0.000	0.000
1.750	0.002	0.001	0.000	0.000	0.000	0.000	0.000	0.000	0.000	0.000	0.000
2.000	0.009	0.007	0.004	0.004	0.004	0.002	0.001	0.001	0.001	0.000	0.000
2.250	0.049	0.054	0.039	0.031	0.023	0.012	0.004	0.003	0.002	0.001	0.000
2.500	0.178	0.201	0.160	0.123	0.080	0.047	0.017	0.007	0.003	0.001	0.000
2.750	0.414	0.416	0.356	0.290	0.179	0.117	0.047	0.014	0.004	0.001	0.000
3.000	0.701	0.606	0.548	0.484	0.296	0.205	0.094	0.024	0.005	0.001	0.000
3.250	0.974	0.746	0.701	0.660	0.410	0.287	0.147	0.036	0.006	0.001	0.000
3.500	1.197	0.857	0.825	0.796	0.508	0.350	0.192	0.049	0.008	0.001	0.000
3.750	1.364	0.960	0.937	0.891	0.587	0.392	0.219	0.060	0.010	0.001	0.000
4.000	1.481	1.067	1.044	0.953	0.648	0.418	0.229	0.069	0.014	0.002	0.000
4.400	1.591	1.248	1.207	1.009	0.717	0.434	0.218	0.079	0.021	0.003	0.000
4.800	1.639	1.429	1.352	1.043	0.755	0.429	0.191	0.081	0.030	0.005	0.000
5.300	1.643	1.636	1.502	1.079	0.760	0.398	0.154	0.076	0.042	0.009	0.001
5.800	1.612	1.816	1.621	1.116	0.724	0.354	0.125	0.069	0.051	0.014	0.001
6.800	1.522	2.119	1.786	1.157	0.599	0.279	0.101	0.059	0.057	0.021	0.001
7.800	1.427	2.239	1.797	1.103	0.490	0.249	0.109	0.059	0.054	0.023	0.002
8.800	1.311	2.012	1.616	0.964	0.413	0.244	0.134	0.063	0.047	0.020	0.001
9.800	1.164	1.565	1.340	0.797	0.350	0.234	0.154	0.065	0.041	0.017	0.001
1.300	0.901	0.991	0.971	0.569	0.261	0.188	0.147	0.058	0.032	0.014	0.001
2.800	0.637	0.690	0.698	0.382	0.175	0.126	0.109	0.047	0.026	0.011	0.001
3.300	0.559	0.630	0.620	0.328	0.151	0.107	0.096	0.043	0.025	0.011	0.001
5.800	0.292	0.440	0.321	0.149	0.069	0.048	0.052	0.031	0.020	0.009	0.001
7.800	0.198	0.334	0.196	0.093	0.044	0.029	0.037	0.027	0.017	0.007	0.001
9.800	0.162	0.262	0.146	0.076	0.036	0.022	0.030	0.025	0.014	0.005	0.001
4.000	0.159	0.212	0.141	0.084	0.041	0.025	0.032	0.023	0.009	0.003	0.000
6.700	0.154	0.205	0.138	0.072	0.041	0.030	0.035	0.020	0.006	0.002	0.000

Figure 10(c)

Figure 11

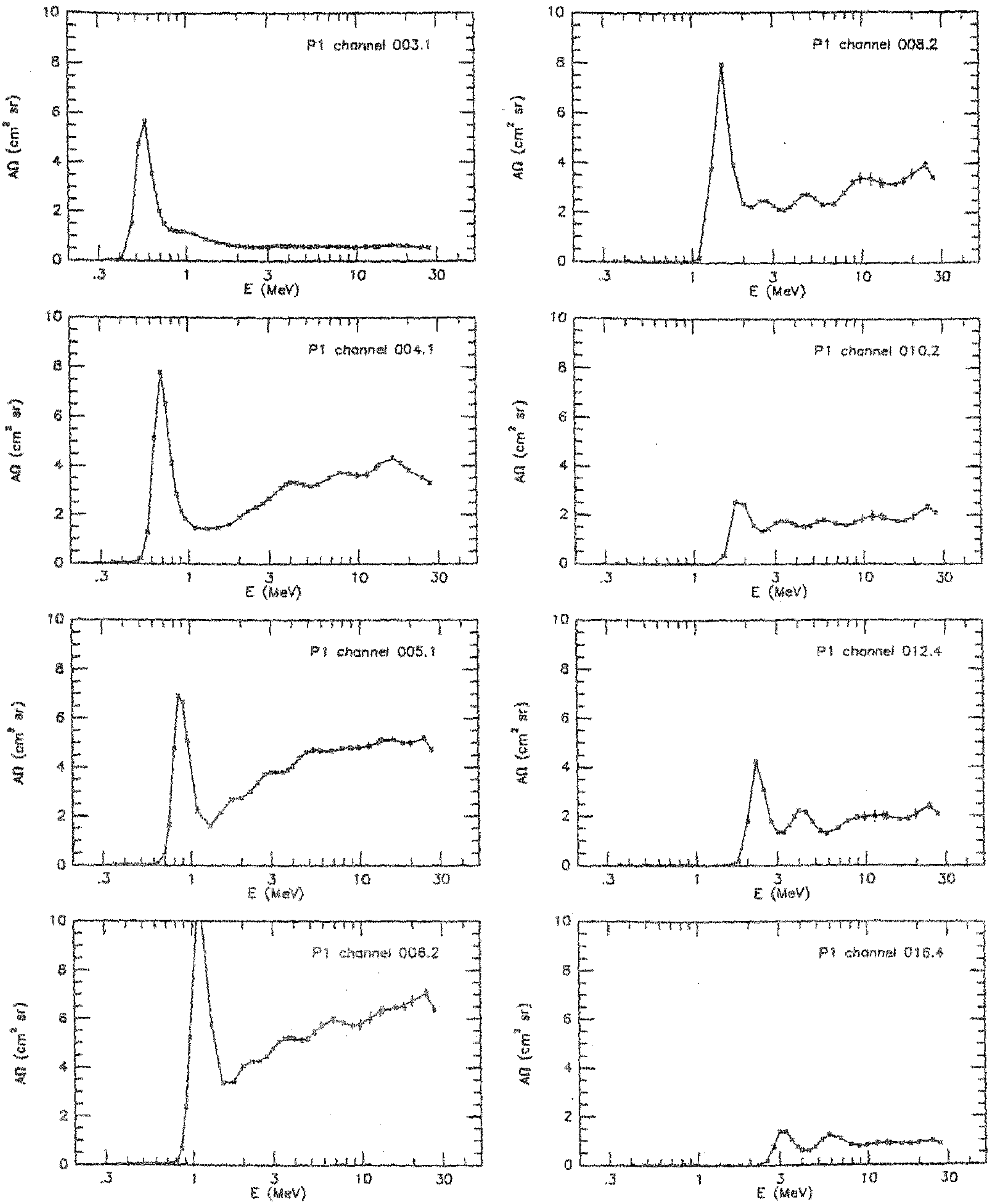
P1 channel 003.1
P1 channel 008.2
P1 channel 004.1
P1 channel 010.2
P1 channel 005.1
P1 channel 012.4
P1 channel 006.2
P1 channel 016.4
AΩ (cm² sr)
E (MeV)

Figure 12(a)

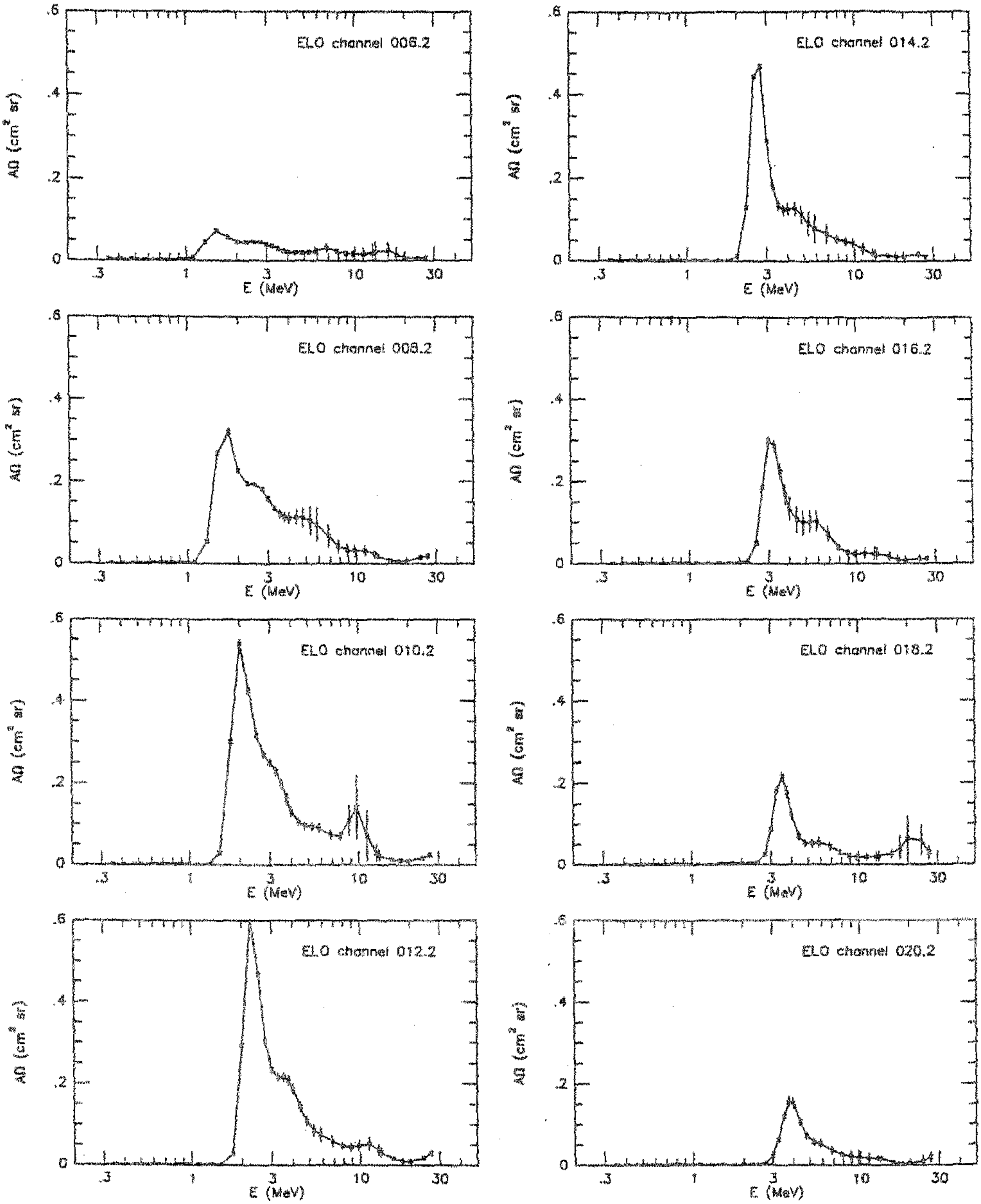
ELO channel 006.2
ELO channel 014.2
ELO channel 008.2
ELO channel 016.2
ELO channel 010.2
ELO channel 018.2
ELO channel 012.2
ELO channel 020.2
AΩ (cm² sr)
E (MeV)
0
.2
.4
.6
.3
1
3
10
30

Figure 14

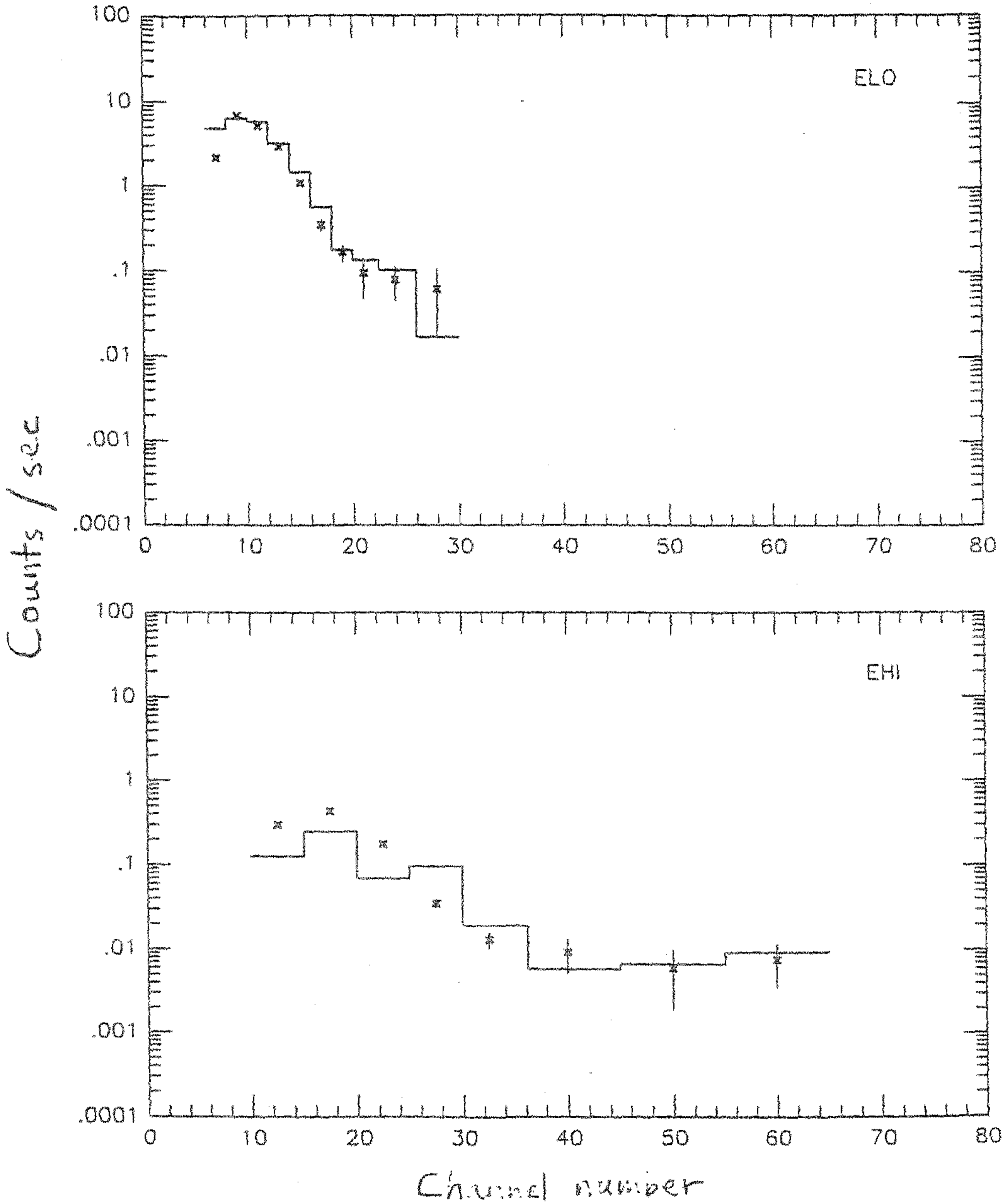

Counts / sec
100
10
1
.1
.01
.001
.0001
ELO
0
10
20
30
40
50
60
70
80
EHI
Channel number

Figure 15

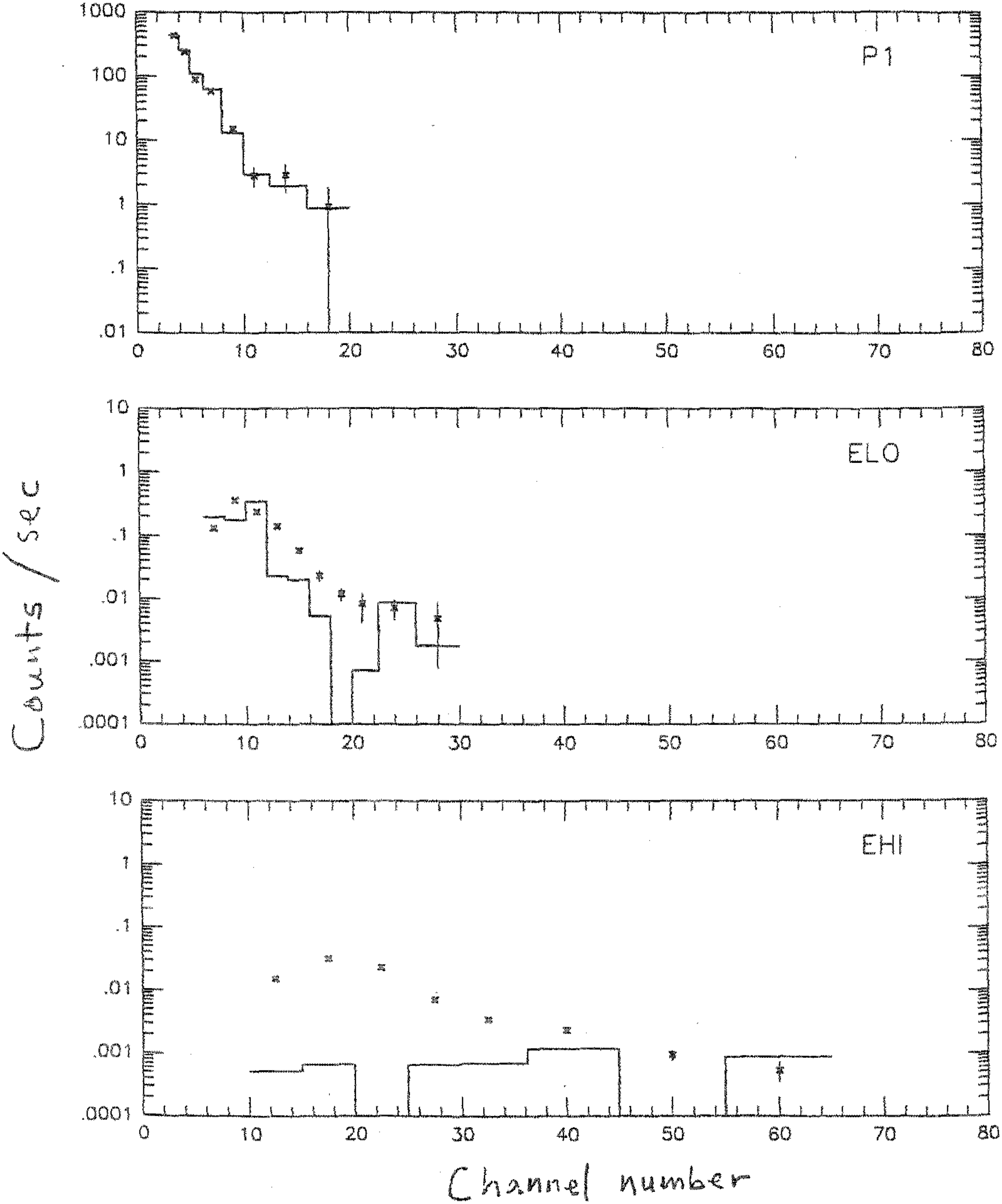
P1
ELO
EHI
1000
100
10
1
.1
.01
.001
.0001
0
10
20
30
40
50
60
70
80
Counts / sec
Channel number

Figure 16

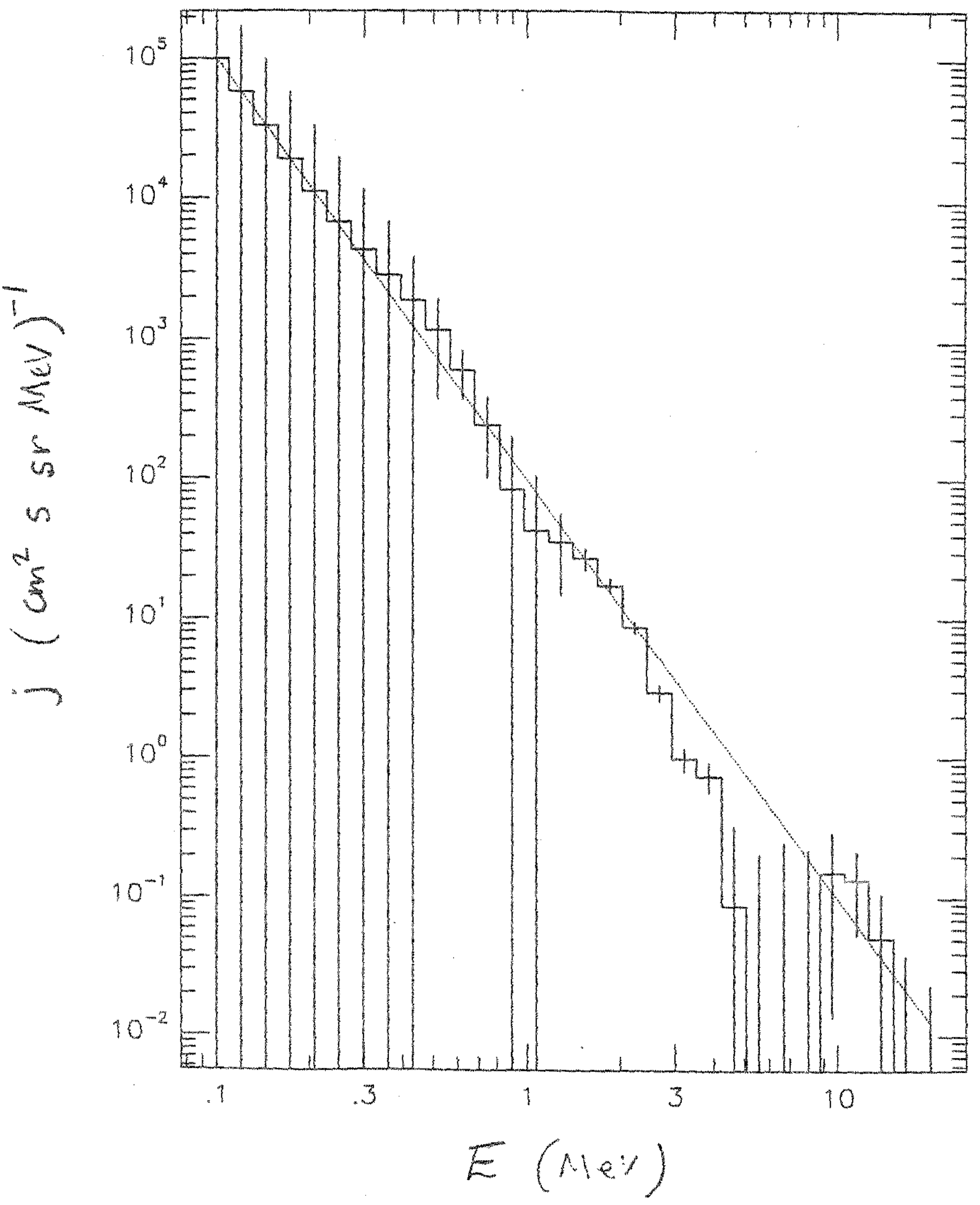

Figure 17

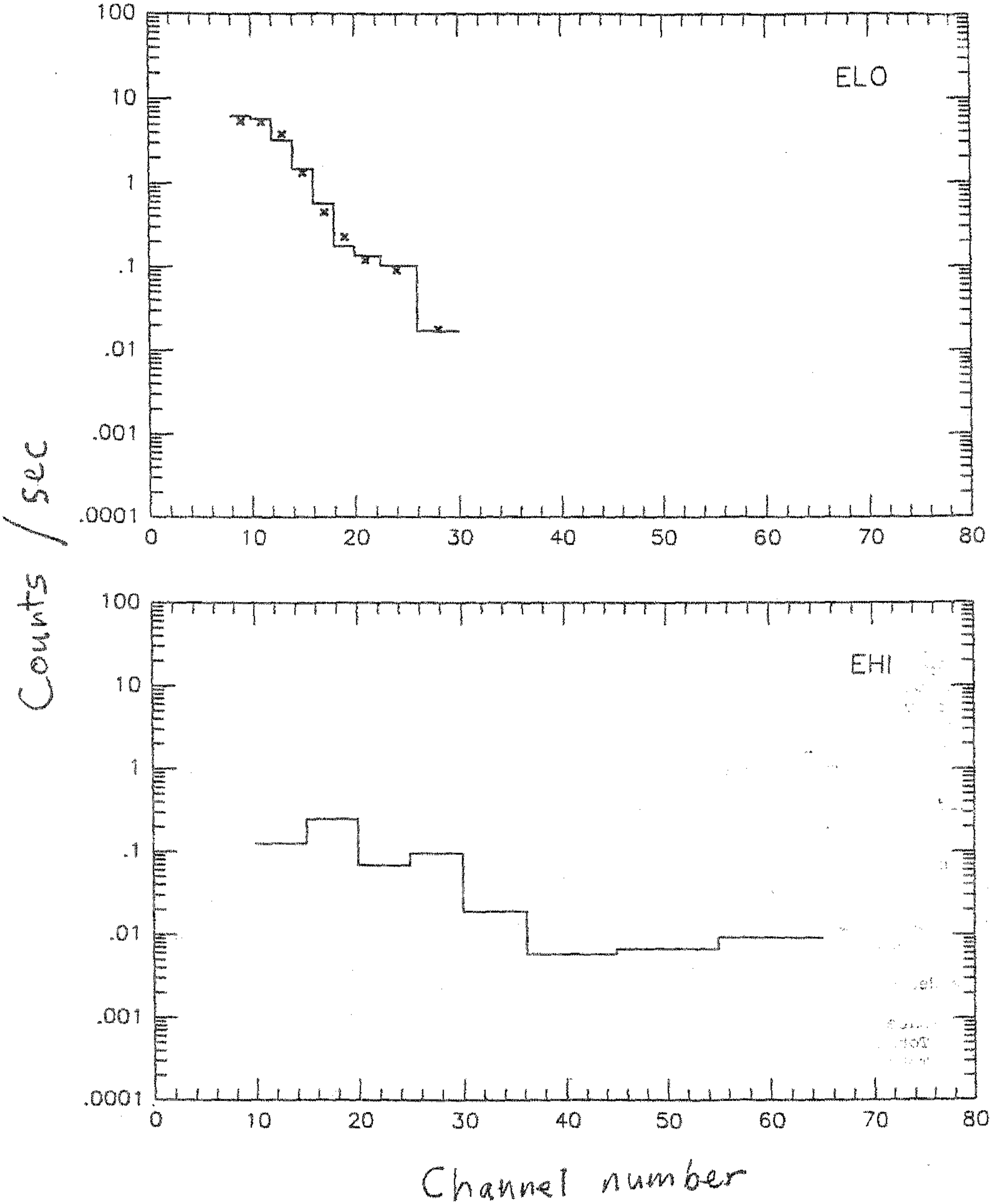
ELO
EHI
100
10
1
.1
.01
.001
.0001
0
10
20
30
40
50
60
70
80
Counts / sec
Channel number

Figure 12

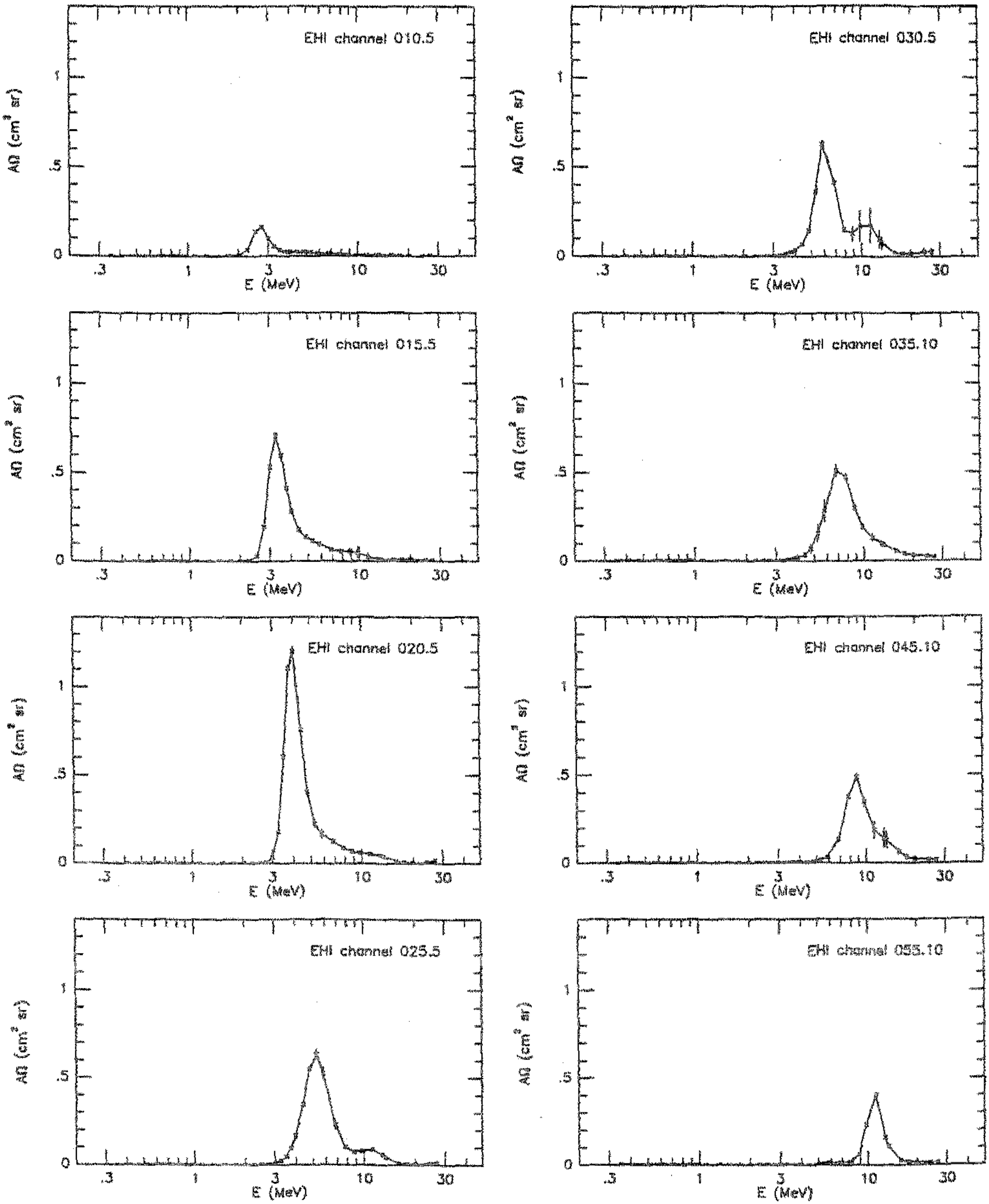
EHI channel 010.5
EHI channel 030.5
EHI channel 015.5
EHI channel 035.10
EHI channel 020.5
EHI channel 045.10
EHI channel 025.5
EHI channel 055.10
AΩ (cm² sr)
E (MeV)
0
.5
1
.3
1
3
10
30

Figure 12(6)

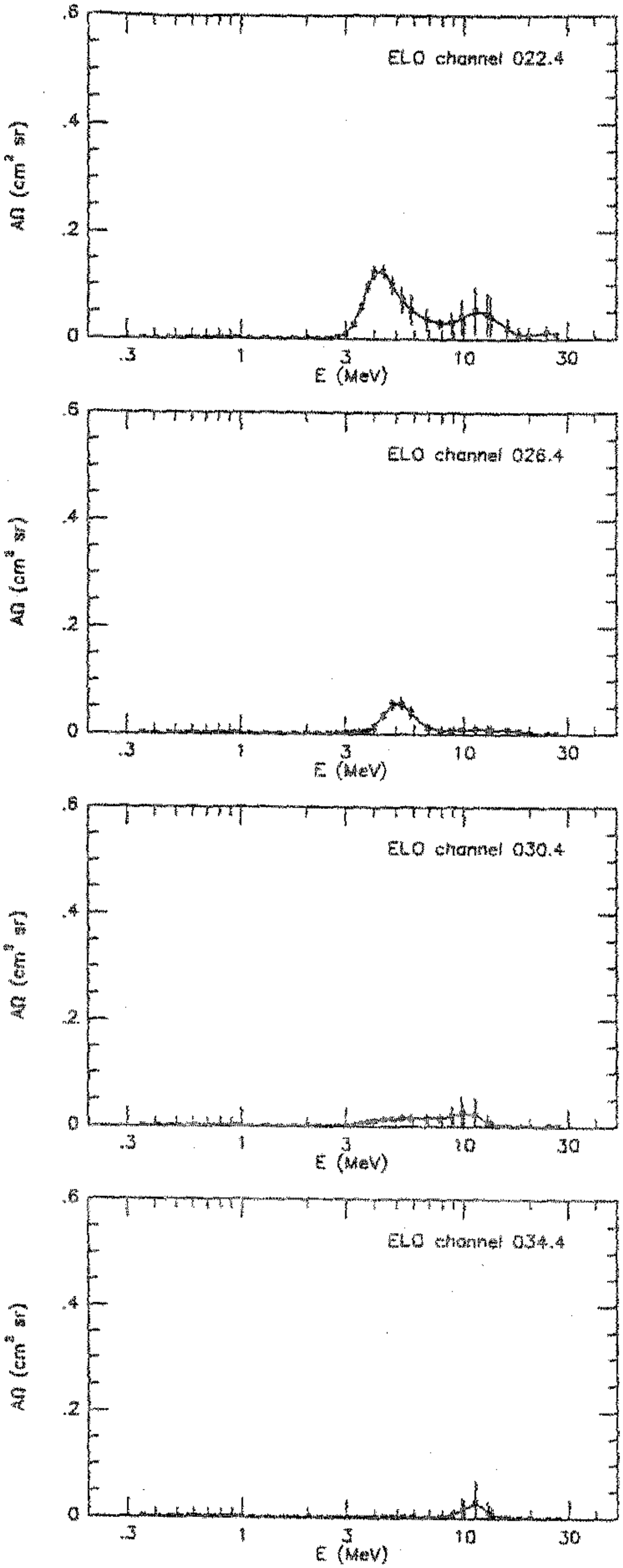
ELO channel 022.4
ELO channel 026.4
ELO channel 030.4
ELO channel 034.4
AΩ (cm² sr)
E (MeV)
.6
.4
.2
0
.3
1
3
10
30